 doi:10.20944/preprints202208.0045.v1

Article

A High-throughput Search for SFXN1 Physical Partners Led to the Identification of ATAD3, HSD10, TIM50 and Subunits of Respiratory Complexes

Nesrine Tifoun [1#], Mourad Bekhouche[1,2#], José M. de Las Heras [1], Arnaud Guillaume [1], Sylvina Bouleau [1], Isabelle Guénal [1], Bernard Mignotte [1,3] and Nathalie Le Floch [1,4*]

[1] LGBC, UVSQ, Université Paris-Saclay, 78000 Versailles, France; nesrine.tifoun2@uvsq.fr (N.T.); jos.de-las-heras-chanes@uvsq.fr (J.M.D.l.H.); arnaud.guillaume@uvsq.fr (A.G.); sylvina.bouleau@uvsq.fr (S.B.); isabelle.guenal@uvsq.fr (I.G.); bernard.mignotte@uvsq.fr (B.M.)
[2] Laboratoire de Biologie Tissulaire et Ingénierie Thérapeutique, UMR5305 CNRS/Université Lyon 1, Lyon, France; mourad.bekhouche@univ-lyon1.fr (M.B)
[3] Ecole Pratique des Hautes Etudes, PSL Research University, 75014 Paris, France;
[4] IUT de Vélizy/Rambouillet, UVSQ, Université Paris-Saclay, 78120 Rambouillet, France
[#] Equally contributed to this work
[*] Correspondence: nathalie.leleu@uvsq.fr

Simple Summary: Mitochondria are central players in cell fate and cell death. Mitochondrial dysfunction is thus seen in many diseases, including neurodegenerative diseases. Mitochondrial activity relies on the presence of numerous mitochondrial transporters. Among these, the sideroflexin family has received little attention to date, despite their emerging importance in human disease. In order to help better understanding their functions and role in human diseases, we wanted to identify molecular partners of one human sideroflexin, namely SFXN1. In this study, we describe the identification of several proteins able to interact with SFXN1, including ATAD3 and HSD10, two mitochondrial proteins that were previously associated with neuronal disorders.

Abstract: Sideroflexins (SFXN) are evolutionarily conserved mitochondrial carriers belonging to the SCL56 family. Until recently, the metabolites transported by SFXN were unknown and they were thought to be transporters of a metabolite involved in iron homeostasis. SFXN1 is now known as the mitochondrial serine transporter. Because little is known about SFXN1 interactome, we launched a high-throughput search of SFXN1 binding partners with the aim to better understand its mitochondrial functions. Using a large-scale identification of SFXN1 physical partners based on co-immunoprecipitation followed by shotgun mass spectrometry (coIP-MS), we identified 96 putative SFXN1 interactants in the MCF7 human cell line. Our *in-silico* analysis of the SFXN1 interactome highlights biological processes linked to mitochondrial organization, electron transport chain and transmembrane transport. Among SFXN1 potential physical partners, ATAD3A and 17β-HSD10, two proteins associated with neurological disorders and neurodegeneration, were further confirmed as interactants using different human cell lines. Further work will be needed to investigate the significance of these interactions in neurological disorders.

Keywords: sideroflexin; SFXN1; mitochondria; ATAD3A; 17beta-HSD10; TIM50

 doi:10.20944/preprints202208.0045.v1

1. Introduction

Sideroflexins are poorly characterized proteins that are evolutionarily conserved among eukaryotes. They belong to the solute carrier SLC56 family, a large family of mitochondrial proteins with 5 members in humans and rodents (SFXN1-SFXN5), 2 members in *Drosophila* (dSfxn1/3 and dSfxn2) and one in yeast (Fungal SideroFlexin 1, FSF1) [1–3]. Their high degree of conservation among eukaryotes suggests that they ensure major mitochondrial functions. Accordingly, loss-of-function mutations in *SFXN4* were described in a rare mitochondrial disease associated with oxidative phosphorylation (OXPHOS) deficiency [4–6]. Downregulation of SFXN1 and SFXN3 in Alzheimer's and Parkinson's diseases was also reported [7,8]. SFXN3, the closest homologue of SFXN1, which is enriched in neurons, may participate in synaptogenesis and maintenance of synapse morphology and has been associated to Parkinson's disease (PD) [9,10]. In *Drosophila*, dSfxn1/3 overexpression counteracts the loss of dopaminergic neurons in a PD model suggesting a neuroprotective role for sideroflexins [11]. Furthermore, *Sfxn3* mutations lead to retinal degeneration in mice [12].

For two decades, SFXN were presumed to be metabolite transporters on the basis of *in silico* structural analysis, but their substrate specificities are still not fully characterized. *S. cerevisiae* homolog Fsf1 (YOR271cp) was proposed to be a candidate alpha-isopropylmalate transporter but no experimental data ascertained this function [13]. Since a mitochondrial iron overload was seen in the flexed-tail mice carrying a mutation in the *SFXN1* gene, it has been thought for a long time that SFXN1 was involved in iron homeostasis. It was thus postulated that SFXN proteins mediate the mitochondrial uptake of a metabolite required for iron metabolism [14]. Indeed, increased mitochondrial iron levels and deficient heme biosynthesis were reported in *SFXN2* and *SFXN4* KO human cells [15,16]. However, the molecular mechanisms that underlie this imbalance in iron homeostasis remain unknown. Recently, in a CRISPR-based screen in human leukemic cancer cells, SFXN1 was identified as the mitochondrial serine transporter thus connecting SFXN1 with the one carbon metabolism (OCM), an essential pathway supporting physiological processes such as the synthesis of purines and amino acid homeostasis [17,18]. The role of SFXN1 in the OCM pathway has provided clues for the regulation of heme biosynthesis by sideroflexins [17]. Indeed, heme biosynthesis relies on the availability of glycine, a precursor of this metabolic pathway, provided by the catabolism of serine. More recently, two studies confirmed the relationships between SFXN1 and heme metabolism. Hence, SFXN1 loss-of-function in mammalian cells and zebrafish leads to an impaired heme biosynthesis [19,20]. Collectively, these data have shed light on the role of the SFXN family in regulating major metabolic pathways and mitochondrial activities. However, despite recent progress in the knowledge of SFXN functions, many questions remain unanswered and little is known about their molecular functions. In particular, their primary role remains largely unknown.

The knowledge of SFXN interactome may help understanding their functions and the mechanisms whereby they regulate mitochondrial activities. When we launched this study, our main objective was to identify SFXN1 binding partners. More specifically, we were interested in uncovering SFXN1 physical partners since SFXN1 is the most conserved member of the SFXN family among eukaryotes and it appears as a main regulator of mitochondrial function through its implication in OCM. Here, we describe the results of our large-scale survey of SFXN1 interactome, obtained following coIP-MS/MS on mitochondria from MCF7 human cells. Notably, we identified two proteins related to neurodegeneration, namely ATAD3 and the multifunctional enzyme 17β-hydroxysteroid dehydrogenase (17β-HSD10). Altogether, these data may help better understanding the role of SFXN1 in pathophysiology and notably in neurological disorders.

Preprints (www.preprints.org) | NOT PEER-REVIEWED | Posted: 2 August 2022 doi:10.20944/preprints202208.0045.v1

2. Materials and Methods

Cell Lines and Cell Culture

HEK-293T, HeLa, HepG2, HT1080, MCF7, MDA-MB-231, MDA-MB-468, MEFSV40, PC12, RKO, and SH-SY5Y cells, were grown in DMEM medium (ThermoFisher, Waltham, MA, USA). KGN, COV434, HCT116 were grown in DMEM/F12 medium (ThermoFisher, Waltham, MA, USA). A2780, A2780Cis, and T47D, cells were grown in RPMI 1640 medium (ThermoFisher, Waltham, MA, USA). All media were supplemented with 10% FBS (ThermoFisher), 1% GlutaMAX (ThermoFisher), 100 μg/ml penicillin and 100 U/ml streptomycin (ThermoFisher). Cells were cultured as monolayers at 37°C in a humidified atmosphere with 5% (v/v) CO_2 and were maintained in culture for no more than 3 months (less than 30 passages).

Plasmids and siRNA transient transfections

Plasmids encoding Flag-SFXNs were obtained from GenScript. Empty vector (pcDNA3.1D V5-His) was obtained from Invitrogen. HEK293T cells were seeded into 60 mm Petri dishes ($1x10^6$ cells / dish) and transfected with 3 μg of DNA using Lipofectamine LTX (Life Technologies, Carlsbad, CA, USA) following manufacturer instructions. For RNAi experiments, MCF7 cells were transiently transfected with either a scrambled control siRNA (Control siRNA-A sc-37007, Santa Cruz Biotechnology, INC) or a pool of specific siRNA for SFXN1 (sc-91814, Santa Cruz Biotechnology, INC). Transfection was done using Interferin™ transfection reagent following manufacturer instructions (Polyplus-transfection Inc., New York, NY). Briefly, a mix of siRNA and Interferin™ transfection reagent was incubated for 10 min at room temperature, added to each well at a final concentration of 10 nM. Cells were incubated at 37°C under standard culture conditions and collected after a 3-, 4- or 7-days to extract proteins.

Protein extraction and subcellular fractionation

For total protein extraction, $2×10^6$ cells were grown in 60 mm dishes, trypsinized 24 hours post-seeding, harvested and centrifuged at 200 g for 5 min. Cell pellets were homogenized in lysis buffer (250 mM NaCl, 50 mM HEPES, 5 mM EDTA, 0.1% NP40, 0.1 M DTT) supplemented with protease 1/100 inhibitors cocktail (Cat.No.04693116001, Roche, Mannheim, Germany) and 0.2 mM sodium orthovanadate/phosphatase inhibitors (cat.567540, Calbiochem, San Diego, CA, USA).

Mitochondria enrichment from mammalian cells and *Drosophila* larvae

For mitochondrial enrichment from human cells, $1.5×10^7$ cells grown on 100 mm dishes were harvested, centrifuged and washed with PBS. Subcellular fractionation by a differential centrifugation method was done as previously [21]. Briefly, cells were harvested, washed in PBS and centrifuged at 200 g for 5 min. Cell pellets were resuspended in fractionation buffer A (250 mM sucrose, 0.1 mM EDTA, 1 mM EGTA, 10 mM Hepes-KOH pH 7,4) and incubated 30 min at 4 °C. Cell disruption was performed by passing the cells through a 26-gauge needle 15 times. The homogenates were centrifuged at 700 g for 15 min at 4 °C to pellet cell debris, nucleus and intact cells. The supernatants were collected and further centrifuged at 7000 g for 20 min at 4 °C to pellet mitochondria. The supernatant was designated as cytosolic fraction. The mitochondria pellets were washed in fractionation buffer B (250 mM sucrose, 5 mM succinate, 5 mM KH_2PO_4, 10 mM Hepes-KOH pH 7,4) and centrifuged at 7000 g for 20 min at 4 °C. Purified mitochondria were lysed in TBS-CHAPS 2% (EUROMEDEX, Strasbourg, France) supplemented with protease inhibitors. All buffers were supplemented with 1 mM protease inhibitors (Roche, Mannheim, Germany). Protein concentration of cell extracts and fractions were determined with a Bradford assay.

Drosophila larvae were dissected in PBS pH 7.6, crushed with a mechanical pestle in 400 μL of fractionation buffer (Tris-HCl 10 mM pH 8, EDTA 10 mM, sucrose 0.32 M), supplemented with a protease inhibitor cocktail (Mini complete without EDTA, Roche). Debris were removed by centrifugation for 5 min at 300 g at 4°C. A sample of supernatant of was kept for further analysis (total extracts). An additional centrifugation was carried out at 2,650 g for 10 min at 4°C. The supernatant was recovered

Preprints (www.preprints.org) | NOT PEER-REVIEWED | Posted: 2 August 2022 doi:10.20944/preprints202208.0045.v1

(cytosolic fraction). The pellet, *i.e.*, mitochondrial fraction, was washed once with fractionation buffer, centrifuged for 10 min at 2, 650g at 4°C and resuspended in 300 µL of fractionation buffer. Samples were denatured with Laemmli buffer 1x, DTT 0.1 M and boiled for 5 min at 96°C and stored at -20°C before Western blot analysis.

Co-Immunoprecipitation

Cells grown in a 100 mm dish were washed thrice in cold PBS. Then, cells were lysed with 1.2 mL NP40 lysis buffer (20 mM Tris, pH 8, 150 mM NaCl, 0.5% NP-40, 0.5% sodium deoxycholate containing a protease inhibitor cocktail (Cat.No.04693116001, Roche, Mannheim, Germany). The lysates were centrifuged at 200 g for 5 min. The supernatant was transferred to a new tube and precipitated with 2 µg anti-SFXN1 or anti-IgG rabbit for negative control. The immune complexes formed were then incubated for 30 min (1000 rpm, 20°C) with G protein-coupled magnetic beads (Bio-Adembeads PAG 0463, Ademtech) previously equilibrated with lysis buffer. The supernatant was collected to ensure the depletion of the immunoprecipitated protein and the pellet was washed 3 times with lysis buffer to remove unspecific binding. For elution, beads were then resuspended with 30 µl of elution buffer (50mM Tris-HCl pH 8.0, 10mM EDTA pH 8.0, 1% SDS) for 4 min at 37 ° C.

Western Blot

Equal quantities of proteins (10 to 30 µg) were loaded on Mini-PROTEAN TGX Stain Free precast polyacrylamide 4–20% gels (BIORAD, Hercules, CA, USA) in 1X Tris Glycine-SDS buffer. Proteins were transferred onto Immobilon-P PVDF membranes (Millipore, Darmstadt, Germany) in 1X Tris Glycine with 20% ethanol. Stain Free technology allows visualizing total proteins adsorbed on the membrane without the use of any dye. For immunoblotting, antibodies were diluted in TBS-Tween 0.1%. Primary antibodies used for immunoblotting are listed in **Table B4**. HRP-coupled secondary antibodies were obtained from Jackson Immunoresearch and Diagomics. Chemiluminescent detection was performed with Clarity Western ECL substrate (BIORAD) and the signal was captured by Chemidoc (BIORAD). Quantification was done using ImageLab software (BIORAD).

Immunofluorescence staining

1 x10^6 cells were plated on 60 mm-diameter Petri dishes containing coverslips and fixed 24 hours post-seeding, at a confluence of 60%, with 3.7 % cold paraformaldehyde (PFA) for 20 min. Cells were washed once with PBS and then permeabilized with 0.5% Tween20 for 30 min. Nonspecific sites were blocked with 1% PBS-BSA for 30 min. immunostaining, cells were incubated for 60 min with primary or secondary antibodies in 3% PBS-BSA. Coverslips were mounted with ProLong Gold Antifade Mountant (Invitrogen). Imaging was performed using Leica TCS SPE or Leica TCS SP8 confocal microscopes (CYMAGES imaging facility, UVSQ). Image analysis was done using ImageJ software.

Imaging and statistical analysis for co-localization

Images were taken in a Leica SP8-X confocal microscope, using a x63 oil immersion objective with 1.4 NA, 1024x1024 resolution and Voxel size x=0.18, y=0.18, z=0.3.

The cell of interest was cropped and properly denoised (background subtracted and filtered with a Gaussian Blur filter) and individual pixel intensity in three consecutive stacks was extracted with FiJi package [22]. Data was processed and graphs generated in Microsoft Excel (2019), R package (R Core Team, 2020) and GraphPad Prism 8.0. Co-occurrence ("Manders' Overlap Coefficient [23]) and correlation ("Pearson's Correlation Coefficient" or "r") values were calculated as reviewed in [24].

Sample preparation for proteomic analyses:

Enriched mitochondrial fraction from MCF-7 cells were prepared as described above. Protein content was estimated by Bradford assay. Proteins (250 µg per condition) were subjected to immunoprecipitation using magnetic beads (Bio-Adembeads, PAG 0463, Ademtech, Pessac, France). Briefly, 250 µg of enriched mitochondrial fraction were incubated in lysis buffer (20 mM Tris pH 8.0, 150 mM NaCl, 0.5% NP40, 0.5% deoxycholate complemented with anti-protease cocktail) supplemented with 2 µg of a

 doi:10.20944/preprints202208.0045.v1

rabbit anti-SFXN1 antibody (HPA063745, Sigma Aldrich, Saint-Quentin-Fallavier, France) or a rabbit IgG control antibody (Cat#12-370, Merck Millipore, Overijse, Belgium) for 30 min at room temperature (RT) at 1000 rpm on a tube rotator. After washing and equilibration in lysis buffer, 20 µL of magnetic beads were added to the immune complex and incubated 30 min under agitation (1000 rpm at RT). The magnetic beads were washed twice in lysis buffer and the bound proteins were then eluted twice using 15 µl of PAG elution buffer (Cat#10701, Ademtech, Pessac, France). The acidic pH was neutralized with 1 volume (30 µl) of 20 mM Tris pH 8.0, 150 mM NaCl and 10 µL of 0.5 M Tris pH 7.5 before sample preparation for MS/MS injection.

Protein extracted from eluates were incubated with 25 mM NH_4HCO_3 buffer containing sequencing-grade trypsin (0.4 µg for 55 µL; Promega) overnight at 37°C. Peptides were desalted using ZipTip µ-C18 Pipette Tips (Millipore). Samples were analyzed using an Orbitrap Q-Exactive Plus, coupled respectively to a Nano-LC Proxeon 1000 equipped with an easy spray ion source (Thermo Scientific, Waltham, MA, USA). On the Q-Exactive Plus instrument, peptides were loaded with an online preconcentration method and separated by chromatography using a Pepmap-RSLC C18 column (0.75 x 500 mm, 2 µm, 100 Å) from Thermo Scientific, equilibrated at 50°C and operated at a flow rate of 300 nl/min. Peptides were eluted by a gradient of solvent A (H_2O, 0.1 % FA) and solvent B (100 % ACN, 0.1% FA), the column was first equilibrated 5 min with 95 % of A, then B was raised to 35 % in 93 min and finally, the column was washed with 80% B during 10 min and re-equilibrated at 95% A during 10 min. Peptides were analyzed in the Orbitrap cell at a resolution of 70,000, with a mass range of m/z 375-1500 and an AGC target of 3.10^6. Fragments were obtained by higher-energy collisional dissociation (HCD) activation with a collisional energy of 28 % and a dynamic exclusion of 30 seconds. MS/MS data were acquired in the Orbitrap cell in a Top20 DDA mode, at a resolution of 17,500, with an AGC target of 2.10^5. Monocharged peptides and unassigned charge states were excluded from the MS/MS acquisition. The maximum ion accumulation times were set to 50 ms for MS and 45 ms for MS/MS acquisitions respectively (Proteomics/Mass Spectrometry Core Facility, Institut Jacques Monod).

Proteomic data analysis

All MS and MS/MS data were processed with the Proteome Discoverer software (Thermo Scientific, version 2.2) coupled to the Mascot search engine (Matrix Science, version 2.5.1). The mass tolerance was set to 6 ppm for precursor ions and 0.02 Da for fragments. The maximum number of missed cleavages was limited to two for the trypsin protease. The following variable modifications were allowed: oxidation (Met), phosphorylation (Ser, Thr, Tyr), acetylation (Protein N-term). The SwissProt database (2017_12 release) with the *Homo sapiens* taxonomy was used for the MS/MS identification step. Peptide identifications were validated using a 1 % FDR (False Discovery Rate) threshold calculated with the Percolator algorithm. High confidence proteins identified in the SFXN1 condition were considered as potential SFXN1 partners if no peptide of the concerned protein was identified in the control condition. The mass spectrometry proteomics data have been deposited to the ProteomeXchange Consortium via the PRIDE [25] partner repository with the dataset identifier PXD030749.

[Reviewer account details:]

Username: reviewer_pxd030749@ebi.ac.uk

Password: X862YIHQ

Biological process analysis using PANTHER

Protein localization was determined using the Gene ontology annotation [26,27]. Proteins identified as partners of SFXN1 were submitted to the online PANTHER classification system using the PANTHER Overrepresentation test (Released 20171205) with the whole annotation for Homo sapiens in the Gene Ontology database as reference set [28]. The overrepresented biological processes with a false discovery rate below 0.05 were assumed to be related to the biological role of the SFXN1. Proteins which

Preprints (www.preprints.org) | NOT PEER-REVIEWED | Posted: 2 August 2022 doi:10.20944/preprints202208.0045.v1

are not binding partners of SFXN1 have also been submitted to the same analysis pipeline to further evaluate the specificity of the biological process determined.

Analysis of SFXN1 interactome using STRING

STRING version 11.0 was used to model SFXN1 interactome with the following basic settings: experiments, database, co-expression and co-occurrence were chosen for active sources; the value for the minimum required interaction score was set at high confidence (0.700) and no more than 5 interactions for the first shell and none for the second shell were parameters chosen for the max number of interactors to show. The network generated can be retrieved with the following permalink: https://version-11-0.string-db.org/cgi/network.pl?networkId=jUrnsUFnafB2 . Functional enrichments for GO terms linked to cellular component permitted to retrieve mitochondrial proteins (GO:0031966), membrane mitochondrial proteins (GO:0005739) and inner membrane mitochondrial proteins (GO:0005743). A Venn diagram was drawn using the web tool accessible here: http://bioinformatics.psb.ugent.be/webtools/Venn/ .

Metascape analysis of SFXN1 physical partners

A list containing the Uniprot identifiers for the 96 proteins found in our co-IP-MS/MS experiment was submitted to the Metascape webtool (https://metascape.org/gp/index.html#/main/step1). Express Analysis was chosen for enrichment and clustering analysis. Metascape Express analysis consists of an automated analysis workflow beginning with identifier conversion and followed by gene annotation, membership search and enrichment analysis. For the meta-analysis done to compare enriched terms related to mitochondrial proteins and SFXN1 partners, we submitted a list of 1484 proteins selected from IMPI database (IMPI-2021-Q4pre) containing 1,357 genes encoding verified mitochondrial proteins with "gold standard" evidence of mitochondrial localization and 127 encoding associated mitochondrial proteins with evidence of mitochondrial localization, but lacking visual confirmation (https://www.mrc-mbu.cam.ac.uk/research-resources-and-facilities/impi).

To construct the protein-protein interaction network for our 96 candidates, Metascape “Express Analysis” mode was chosen. It utilizes the “Physical Core” dataset which contains only the 2/3 of higher-scoring corresponding STRING data. The MCODE algorithm automatically extracted densely-connected protein complexes from our list of SFXN1 partners.

Oxygen Consumption Rate measurement

Respiration was assessed in live cells using Seahorse XF HS mini Analyzer (Agilent Technologies). The oxygen consumption rate (OCR) was determined with Seahorse XF Cell Mito Stress Test Kit (Agilent Technologies #103015) according to the manufacturer's instructions. Before the assay, 4×10^5 of MCF7 cells were transfected in suspension in a 6-well plate with a scrambled siRNA (Control siRNA-A: sc-37007, Santa Cruz Biotechnology) or a pool of three SFXN1 siRNA (SFXN1 siRNA (h): sc-91814, Santa Cruz Biotechnology). Cells were trypsinized 48 hours post-transfection and 2.5×10^5 cells/well were plated on a polylysine-coated Seahorse XFp cell culture miniplate in Seahorse XF DMEM supplemented with 1mM pyruvate, 2 mM glutamine and 10 mM glucose. Following a 1-hour incubation at 37°C without CO_2, the plate was loaded into the Seahorse XF HS mini Analyzer, and the OCR was measured during sequential addition of 1.5 µM oligomycin, 1 µM carbonylcyanide m-chlorophenylhydrazone (FCCP), 0.5 µM antimycin A plus rotenone.

Proximity ligation assay

Proximity ligation assay experiment was done with the Duolink® In Situ Red Starter Kit according to the manufacturer instructions (DUO92101, Sigma Aldrich, Saint-Quentin-Fallavier, France) on MCF-7 cells and using mouse anti-HSD10 antibody (sc-136326, Santa Cruz Biotechnology, Dallas, U.S.A.) and rabbit anti-SFXN1 antibody (HPA063745, Sigma Aldrich, Saint-Quentin-Fallavier, France). A negative control without primary antibodies was done. Briefly, MCF-7 cells were cultured on coverslips in 6-well plates. Cells were washed 3 times with PBS, fixed 10 min in 3.7% PFA

 doi:10.20944/preprints202208.0045.v1

and permeabilized 10 min with 0.1% Triton X-100 at 37°C. The cells were washed thrice for 5 min with PBS between each step. The coverslips were placed in a humidified chamber and blocked with 50 µL Duolink blocking solution for 60 min at 37°C. Primary antibodies at 2 µg/ml were incubated overnight at 4°C. After 2 washes for 5 min with the provided wash buffer A, PLA probes were added and incubated for 1h at 37°C in a humidified chamber. After 2 washes of 5 min with wash buffer A, the ligase (diluted 1/40 in ligation buffer) was incubated 30 min at 37°C. The coverslips were washed again twice 5 min with buffer A and the amplification step in the presence of the DNA polymerase was performed during 100 min at 37°C in the dark. Coverslips were washed twice for 10 min with buffer B, then nuclei were stained with DAPI for 15 min and the cover-slips were mounted in ProLong Gold Antifade Mountant (Invitrogen). Slides were observed using a Leica TCS SPE confocal microscope with the DAPI and TRITC filters. The number of red dots was quantified using FIJI software and the Cell Counter plug-ins [22].

Biological resources:

The lists of antibodies, cell lines and plasmids used in this study are given as supplemental material in Appendix A. The RRID portal (https://scicrunch.org/resources) was used to provide antibodies identifiers [29].

3. Results

3.1. SFXN1 is an evolutionarily conserved mitochondrial protein widely distributed over human cell lines

To identify cell lines suitable for the search of SFXN1 physical partners, we first compare SFXN1 levels in different human cells. SFXN1 was easily detected by Western blot in the cell extracts obtained from human transformed or tumor-derived cell lines (**Figures 1a-b**). We also tested our SFXN1 antibody in rat and *Drosophila*, two widely used organism models. Rat SFXN1, as well as dSfxn1 / dSfxn2, the two *Drosophila* sideroflexins, were successfully detected (**Figures 1c-d**). The specificity of our anti-SFXN1 antibody was confirmed using RNA interference to deplete SFXN1 (**Figure A1**). Evidence for a mitochondrial localization of sideroflexins exist in the literature [4,9,15,17] and the mitochondrial localization of SFXN1 to the inner mitochondrial membrane has been recently confirmed [19]. Here, we analyzed SFXN1 content in mitochondria-enriched fractions. As expected, SFXN1 is found in mitochondria-enriched fractions from MCF7, A2780, COV434 and PC12 cells, as well as in mitochondrial fractions obtained from *Drosophila* larvae (**Figures 1d-e and A2**). Endogenous SFXN1 and exogenous Flag-tagged SFXN1 were also shown to colocalize with mitochondria in our immunofluorescence studies, further confirming the mitochondrial localization of SFXN1 (**Figure 1f and A2-A3**). This is in agreement with the data available in the Human Atlas Protein database [30], where a punctate pattern resembling that of mitochondria, is seen using a specific antibody raised against the C-terminus of SFXN1 which is predicted to be in the intermembrane space of mitochondria [31] (**Figure A4**).

Preprints (www.preprints.org) | NOT PEER-REVIEWED | Posted: 2 August 2022 doi:10.20944/preprints202208.0045.v1

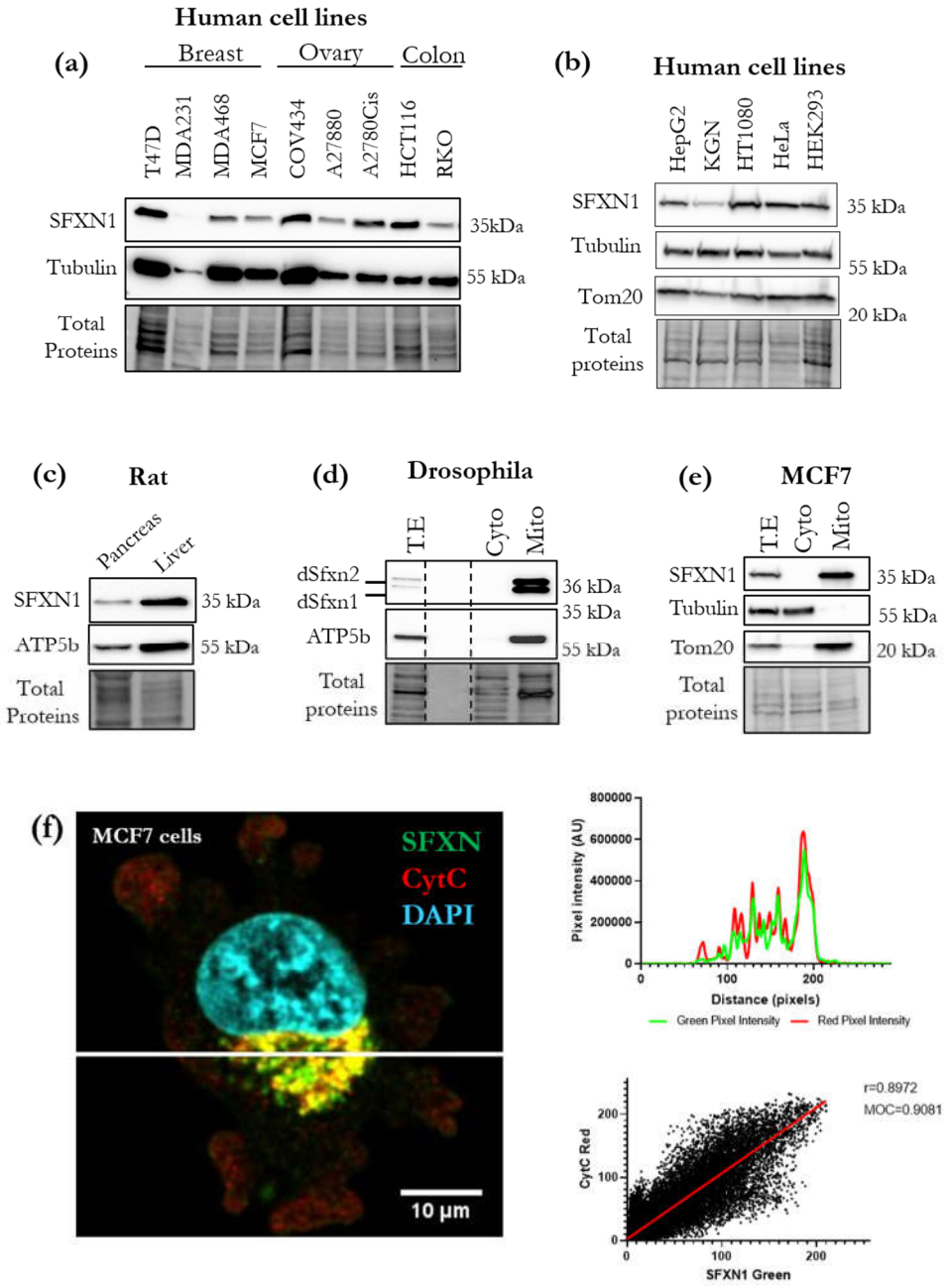

Figure 1. SFXN1 is a mitochondrially-localized protein that is highly abundant in human cell lines. (**a,b,c**) Western blot analysis of SFXN1 levels in commonly used human cell lines or rat tissues. Total proteins were detected using stain free imaging of the membrane before SFXN1, tubulin, Tom20 and F1F0-ATPase (β subunit) revelation. Levels of the tubulin, the mitochondrial import receptor subunit Tom20 and the β subunit of the mitochondrial ATP synthase (ATP5b) serve as a loading control. (**d,e**) Cell fractionation was performed on cell extracts from wild type drosophila larvae (**d**) and MCF-7 cells (E). Total extracts (T.E), cytosolic (Cyto) and mitochondrial (Mito) fractions were subjected to immunoblot analysis with an anti-SFXN1 (Sigma-Aldrich Cat# HPA019543, RRID:AB_1856789). An anti-F1-F0 ATPase (β subunit) or an anti-Tom20 were used to control the mitochondria enrichment. (**f**) Sum projection of three consecutive stacks of MCF7 cell with SFXN1 (green) and Cytochrome c (red) mitochondrial labeling on the left. One cell is shown, see appendix A (**Figure A2c**) for the whole field. Signal distribution profile of green and red pixels, corresponding to the white horizontal bar on the left image, is shown on the right (upper panel), with highly similar behaviors. Correlation of all pixels corresponding to three individual stacks projected are also presented (on the right, lower panel). Pearson Correlation coefficient (r) is shown; correlation is highly significant ($p<0.0001$ two-tail test). Manders's Overlap Coefficient (MOC) is also expressed. Both values, r and MOC, being high, indicate a strong and significant colocalization between SFXN and Cyt C staining.

 doi:10.20944/preprints202208.0045.v1

3.2. Identification of SFXN1 partners by coIP-MS/MS

To obtain clues on SFXN1 mitochondrial functions and interactome, we launched a high-throughput search for SFXN1 physical partners. The MCF7 human cell line was chosen because of its high SFXN1 content and its ease to propagate allowing the recovery of the large number of cells needed for fractionation and mitochondrial enrichment. First, SFXN1 was immunoprecipitated from mitochondria-enriched extracts of MCF7 cells. Co-precipitated proteins were identified by tandem mass spectrometry (MS/MS). To ensure the specificity of the interactions, we also performed a control IP with an irrelevant IgG (**Figures 2a and A5**). The comparison of the proteins identified in the SFXN1-IP and IgG-IP allowed us to establish a list of 96 candidates. We further analyzed our list of SFXN1 binding partners using STRING and found that 33 partners were annotated as mitochondrial proteins among which 23 are proteins from the inner mitochondrial membrane (**Figure 2b** and **Table B1**). Of note SFXN1, SFXN2, SFXN3 and SFXN5 were not annotated as proteins from the inner mitochondrial membrane.

Biological processes related to SFXN1 partners were then identified using Panther (**Figure 2c**, **Tables B2 and B3**). Among these, electron transport chain (ETC) is significantly enriched, with 7 proteins specifically found in the SFXN1-IP. As shown in **Table B3**, 3 subunits of the complex I (TIMMDCI from the ND1 module, MT-ND2 and NDUFA10 from the ND2 module), 3 subunits over the 13 forming the complex IV (Cytochrome c oxidase subunit 6A1, Cytochrome c oxidase subunit 6C and Cytochrome c oxidase subunit 7A2) and Cytochrome c oxidase assembly protein COX11 were co-immunoprecipitated with SFXN1. These results suggest a physical proximity between SFXN1 and the ETC.

Preprints (www.preprints.org) | NOT PEER-REVIEWED | Posted: 2 August 2022 doi:10.20944/preprints202208.0045.v1

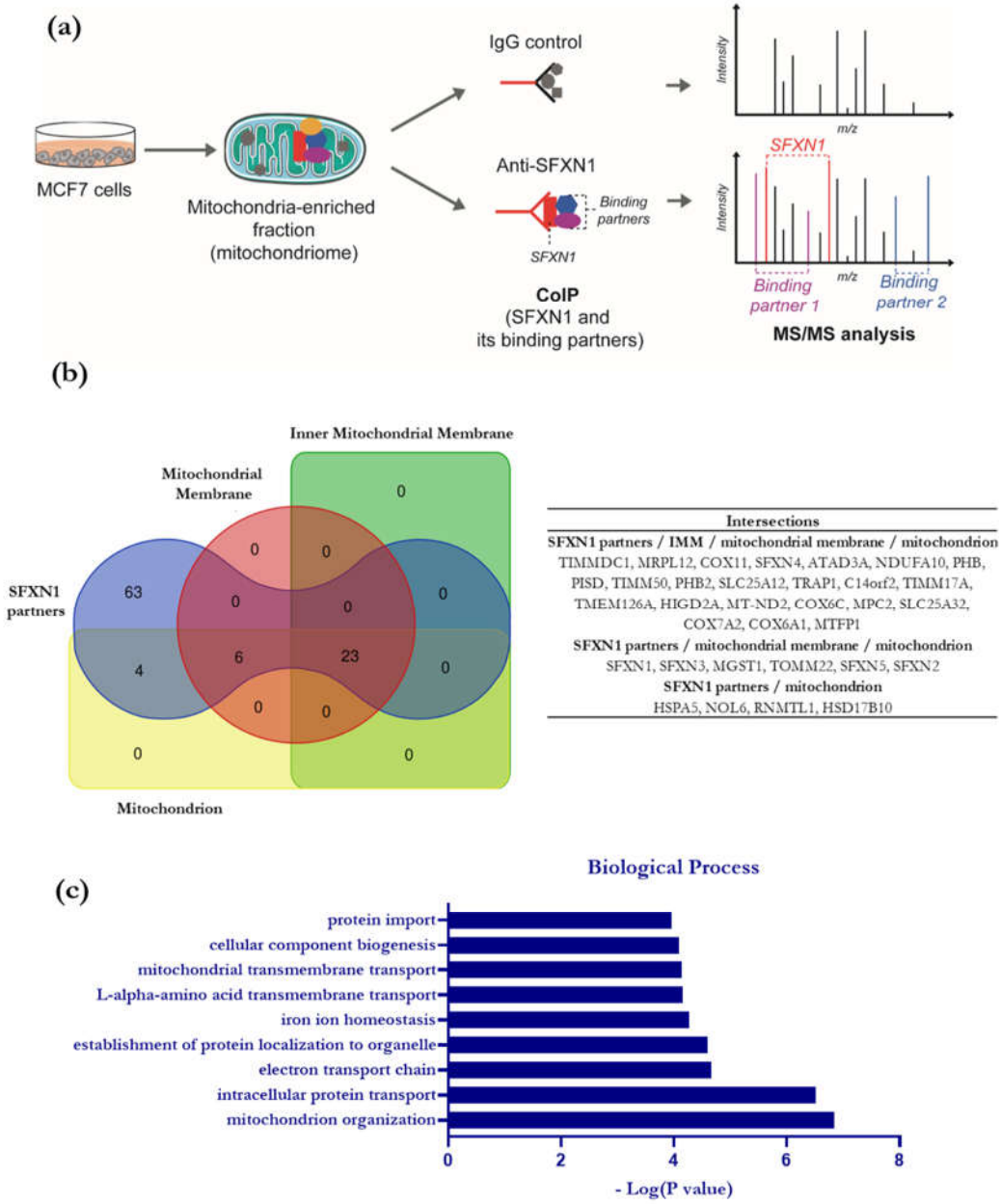

Figure 2: High-throughput search for SFXN1 physical partners (CoIP-MS) and related biological pathways. (**a**) Scheme of the methodology chosen to identify SFXN1 binding partners. An anti-SFXN1 antibody (Atlas Antibodies Cat# HPA063745, RRID:AB_2685111) was used to co-immunoprecipitate SFXN1 and its binding partners from MCF7 derived mitochondrial fractions. A control IP was done using a rabbit IgG. Proteins identified by MS/MS that were not found in the control condition were assumed as potential SFXN1 binding partners. (**b**) Venn diagram showing the overlaps between the lists of SFXN1 partners and of mitochondrial proteins identified by MS/MS. Mitochondrial proteins were identified based on the Gene Ontology Annotation tool. (**c**) Biological processes related to the potential partners of SFXN1 determined using PANTHER Overrepresentation test.

Preprints (www.preprints.org) | NOT PEER-REVIEWED | Posted: 2 August 2022 doi:10.20944/preprints202208.0045.v1

3.3. In silico analysis of the interactome of SFXN1

3.3.1. STRING analysis

Physical partners listed in **Table B1** were analyzed using the STRING v11.0 software [32]. The SFXN1 network shows three strong clusters, one of them containing SFXN1 (**Figure 3).** Functional enrichment analysis identified Gene Ontology (GO) terms related to oxidative phosphorylation, ribosome, RNA binding and transporter activity (**Figures A6 and A7**). Interestingly, this analysis confirmed the physical interaction between SFXN1 and Tim50, which was previously observed in large-scale studies.

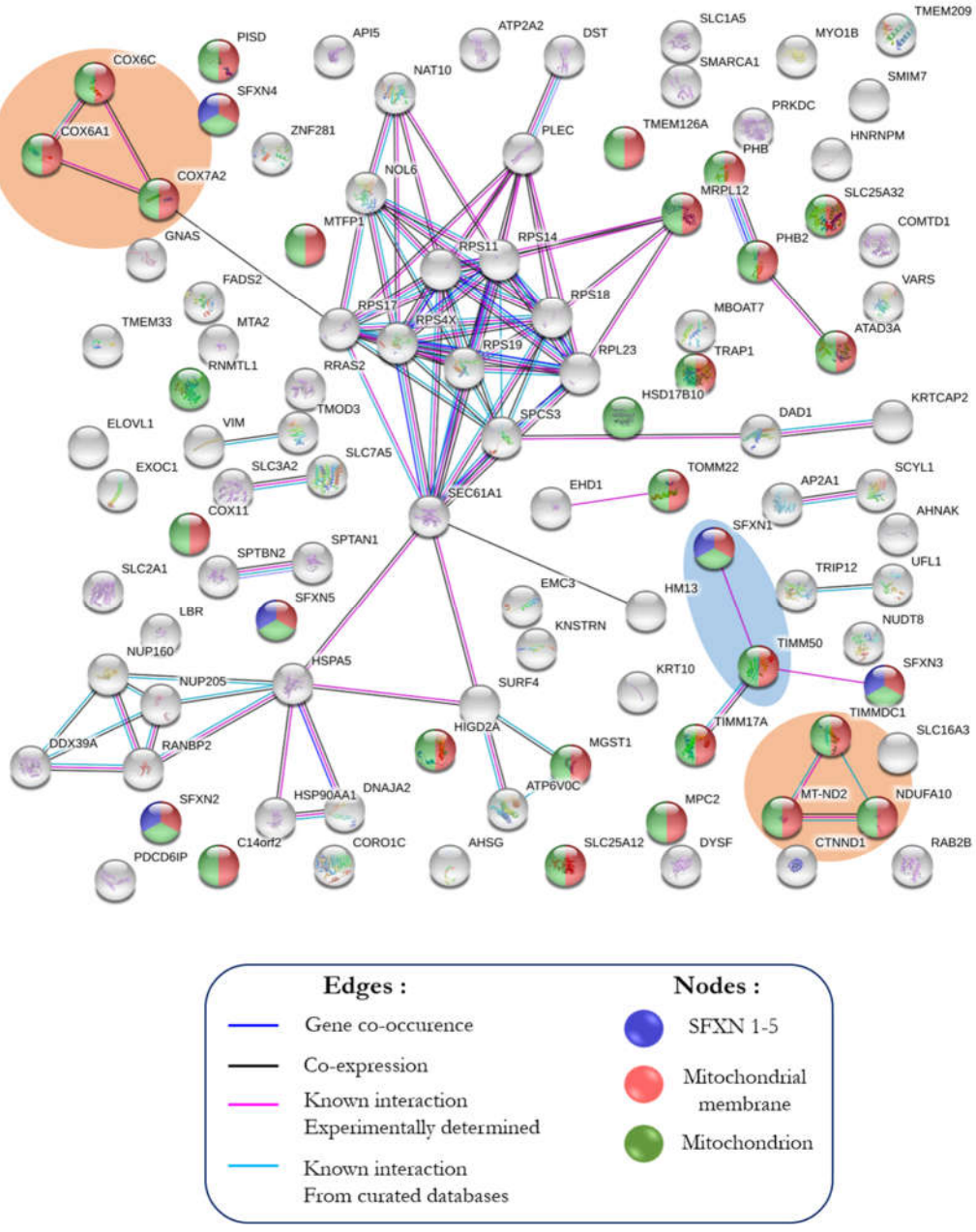

Figure 3: Analysis of the SFXN1 interactome using STRING. STRING protein-protein interaction network (https://string-db.org) was constructed for physical partners found in our Co-IP/MS/MS experiment. Two strong clusters are found between proteins of the electron transfer chain (complex I and IV, in the orange areas) and one cluster involving TIMM50 and SFXN1 is highlighted (in the blue area). SFXN family members, mitochondrial proteins and mitochondrial membrane proteins are colored in blue, green and red, respectively.

Preprints (www.preprints.org) | NOT PEER-REVIEWED | Posted: 2 August 2022 doi:10.20944/preprints202208.0045.v1

3.3.2. Metascape analysis

- Enrichment analysis and Clustering

The web-based portal tool Metascape was used to facilitate the interpretation of our data [33]. Metascape Express analysis consists of an automated analysis workflow beginning with identifier conversion and followed by gene annotation, membership search and enrichment analysis. Automated analysis of gene annotations using Metascape Express analysis permitted to identify significantly enriched terms linked to our 96 candidates. Top 20 enriched clusters are shown in **Figure 4.** Interestingly, the top 3 enriched clusters are related to mitochondrial transmembrane transport, mitochondrion organization and mitochondrial respiration.

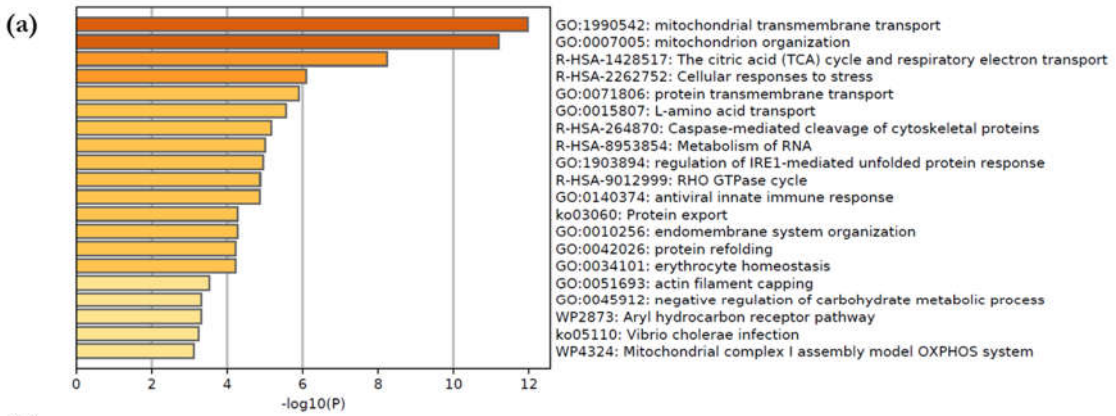

Figure 4. Metascape Enrichment analysis for SFXN1 partners. (a) Metascape bar graph for viewing top non-redundant enrichment clusters, one per cluster, using a discrete color scale to represent statistical significance (dark orange for the most significant clusters). **(b)** Hits from the top 3 enrichment clusters (mitochondrial transmembrane transport, mitochondrion organization, TCA cycle and respiratory chain).

Because we immunoprecipitated SFXN1 from mitochondria enriched fractions, it is not really surprising to retrieve processes related to mitochondrial functions. Thus, we next tried to identify the processes related to mitochondrial functions that are preferentially enriched in our experimental dataset. For this purpose, a Metascape meta-analysis was done to compare enriched terms associated with SFXN1 partners and those related to proteins known to be mitochondrial. As shown in **Figure 5**, among the most significant clusters related to mitochondrial proteins, five clusters are significantly enriched for SFXN1 partners: mitochondrial transmembrane transport, respiratory electron transport, mitochondrial complex IV assembly, mitochondrial protein import, mitochondrial transport. Thus, SFXN1 physical partners identified in this study appear to be mainly involved in respiration and mitochondrial transport.

Preprints (www.preprints.org) | NOT PEER-REVIEWED | Posted: 2 August 2022 doi:10.20944/preprints202208.0045.v1

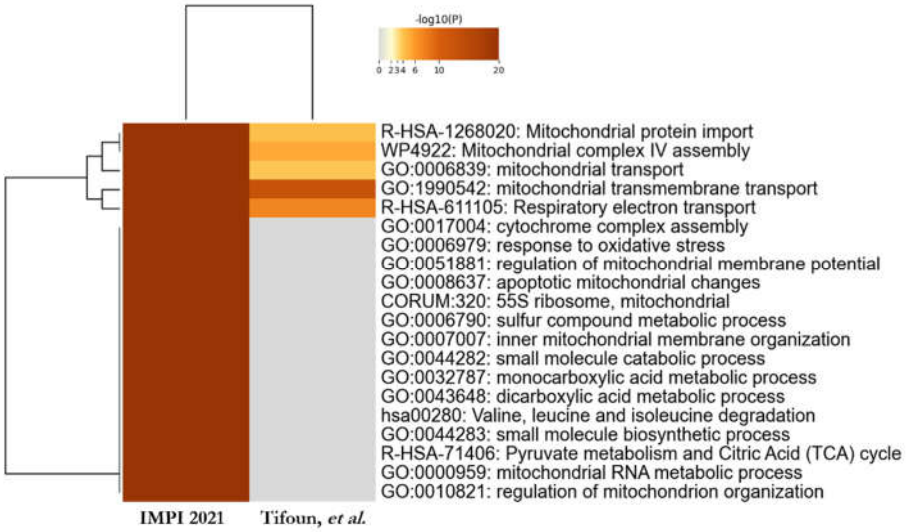

Figure 5. Comparison of top 20 enriched terms related to mitochondrial proteins and SFXN1 partners. Heatmap of enriched terms across input gene lists, colored by p-values (grey cells indicate the lack of enrichment for that term in the corresponding gene list).

- Protein-protein interactome network analysis using Metascape

Metascape was utilized to automatically construct SFXN1 protein-protein network from our list of putative SFXN1 physical partners based only on physical interactions available in BioGrid, OmniPath, InWeb_IM and STRING databases. The protein interaction network formed by the putative SFXN1 physical partners is shown in **Figure 6.** Four densely connected protein complexes were identified and among them three were functionally labeled. SFXN1 and SFXN3 were found in two separate MCODE complexes respectively related to protein folding and mitochondrial transport. SFXN1 and ATAD3A were found in the same densely connected complex highlighting the existence of a physical interaction between SFXN1 and ATAD3A, in agreement with our mass spectrometry analysis.

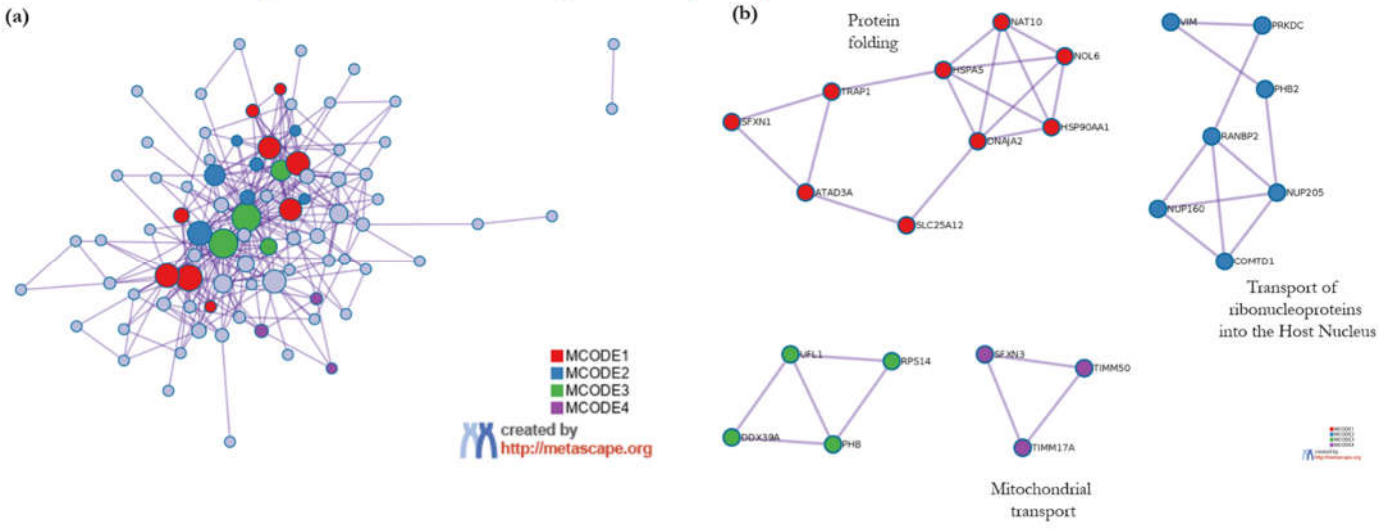

Figure 6: **(a)** Metascape visualization of the network formed by SFXN1 partners identified in our IP-MS/MS experiment. Densely-connected complexes identified by the MCODE algorithm are colored according to their identities. **(b)** Four MCODE protein complexes extracted from the SFXN1 network. Functional annotations based on the top-three functional enriched terms were available for MCODE1, MCODE 2 and MCODE4 complexes.

Preprints (www.preprints.org) | NOT PEER-REVIEWED | Posted: 2 August 2022 doi:10.20944/preprints202208.0045.v1

3.4. Comparative study to identify highly probable SFXN1 partners

With the aim to identify highly probable SFXN1 physical partners, we further utilized Metascape to compare our list of physical partners with the data from a BioID study in which SFXN1 was used as a bait and gave a list of 130 interactants [34]. Our comparative analysis highlighted ten proteins shared by the two lists including SFXN1, and among them were found SFXN2, 17β-HSD10, three mitochondrial translocases and the two metabolite carriers SLC25A12 and SLC1A5 (**Figure 7**). SLC25A12, also known as Aralar, is a calcium-binding mitochondrial carrier protein and is involved in the exchange of cytosolic aspartate for mitochondrial glutamate across the inner mitochondrial membrane [35]. SLC1A5 is a neutral amino acid transporter located in the plasma membrane. Thus, it was quite surprising to find this carrier as a shared protein. However, it was recently shown that a novel variant of the SLC1A5 gene, transcribed from its alternative transcription initiation site was targeted to the mitochondria. This SCL1A5 variant is a mitochondrial glutamine transporter that is also able to mediate alanine and serine uptake *in vitro* [36,37].

Of note, whereas ATAD3A was identified in our study, it is ATAD3B instead that was found in the study of Liu *et al*. As well, TMEM126B, a complex I assembly factor, but not TMEM126A was shown to interact with SFXN1 using the BioID approach. Maybe these discrespancies could be explained by shared peptides detected in mass spectrometry experiments.

Since SFXN1 was recently described as the mitochondrial transporter of Serine linking SFXN1 to one carbon metabolism, it is interesting to find Serine Hydroxy Methyl Transferase 2 (SHMT2) in Liu's list of putative SFXN1 partners. SHMT2 is the main mitochondrial enzyme of the OCM pathway catabolizing Serine into Glycine following its entry inside the mitochondrion. However, we did not find this protein in our list of candidates.

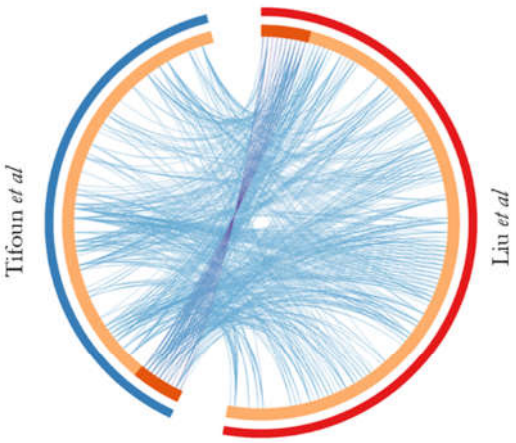

Uniprot ID	Gene symbol	Description
O60884	DNAJA2	DnaJ heat shock protein family (Hsp40) member A2
Q9BW72	HIGD2A	HIG1 hypoxia inducible domain family member 2A
O75746	SLC25A12	solute carrier family 25 member 12
Q99714	HSD17B10	hydroxysteroid 17-beta dehydrogenase 10
Q9NS69	TOMM22	translocase of outer mitochondrial membrane 22
Q9NPL8	TIMMDC1	translocase of inner mitochondrial membrane domain containing 1
Q15758	SLC1A5	solute carrier family 1 member 5
Q9H9B4	SFXN1	sideroflexin 1
Q3ZCQ8	TIMM50	translocase of inner mitochondrial membrane 50
Q96NB2	SFXN2	sideroflexin 2

Figure 7: Circos plot showing overlapping genes from this study and Liu et al. On the outside, each arc represents a gene list. On the inside, dark orange color represents the genes that are shared by the two lists and light orange color represents genes that are unique to a gene list. Purple lines link the same gene that is shared by the two lists. Blue lines link different genes that fall under the same ontology term. The table gives the list of shared genes.

 doi:10.20944/preprints202208.0045.v1

To identify pathways that are enriched both in Liu dataset and ours, we further analyzed the meta-analysis results obtained with Metascape. Ten enrichment clusters are shared between the two lists, the most significant ones being related to mitochondrial respiration, mitochondrion organization and mitochondrial transport (**Figure 8a**). Protein-protein interaction network was automatically constructed from a merge list including SFXN1 partners identified in both studies and MCODE components were identified from the merged network (**Figure 8b**). Five shared genes are seen in the densely-connected networks given by Metascape. SFXN1 was found in a dense network described by the GO term "inner mitochondrial membrane organization", together with SLC25A12 and TOMM22.

Preprints (www.preprints.org) | NOT PEER-REVIEWED | Posted: 2 August 2022 doi:10.20944/preprints202208.0045.v1

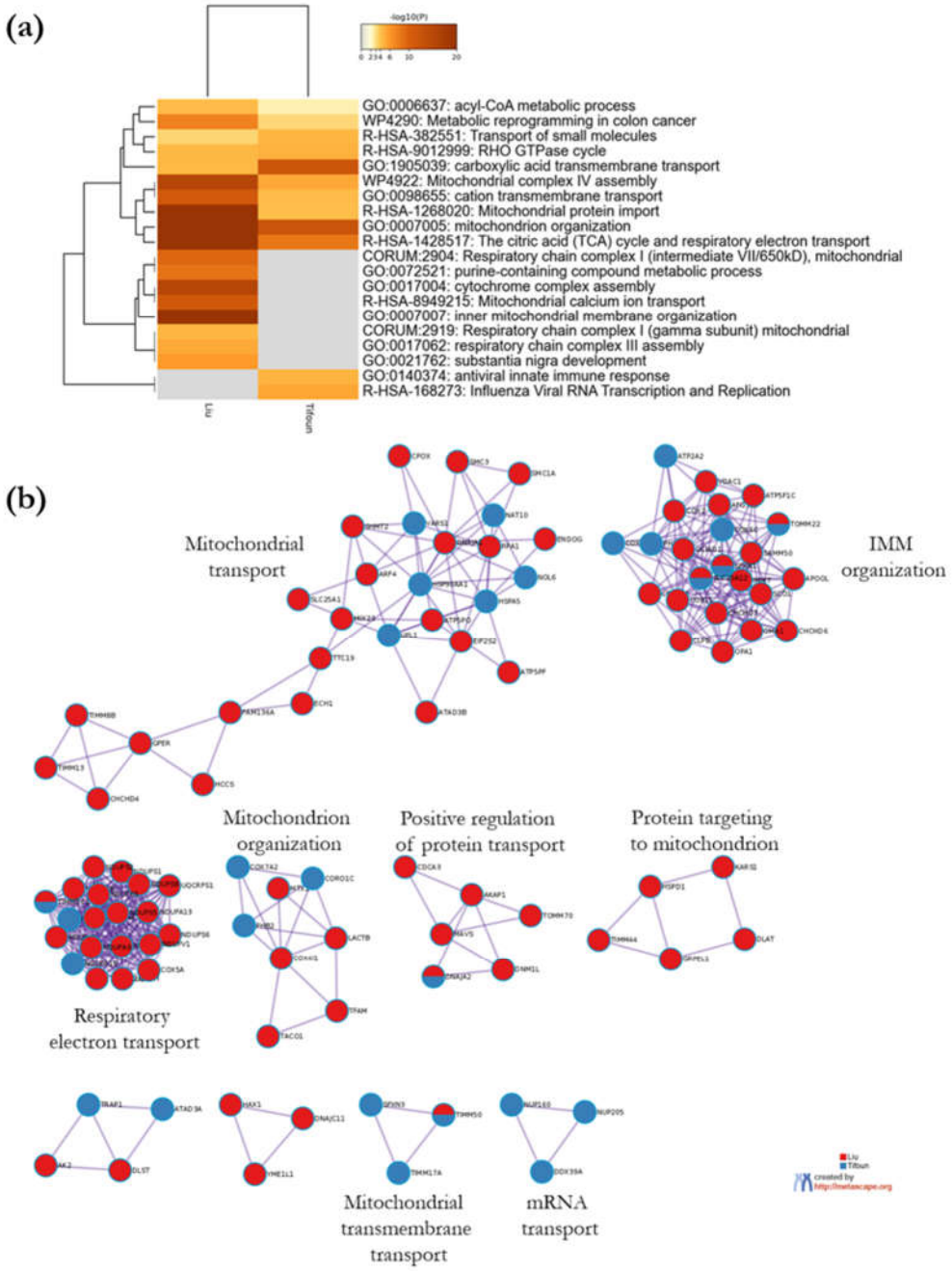

Figure 8: Visualization of the meta-analysis results based on the two lists of SFXN1 binding partners. **(a)** Heatmap showing the top enrichment clusters colored according to their significance. The term with the best p-value within each cluster is given as its representative term. **(b)** Metascape visualization illustrating densely-connected protein-protein interaction networks automatically identified from the merged lists of SFXN1 physical partners. A representative GO term was chosen between the top three best p-value terms to depict each MCODE network, when available. Network nodes are displayed as pies. Color code for pie sector represents a gene list (Blue for our list, red for Liu list).

3.6. ATAD3, 17-beta-HSD10, TIM50 and NDUFA10 physically interact with SFXN1

We then wanted to confirm the interaction between SFXN1 and candidates of particular interest and we first considered those with a high Mascot's score. Because SFXN1 levels may be decreased in neurodegenerative diseases and its closest homologue SFXN3 may regulate synaptic morphology [7,9] , we focused on candidate proteins that have been linked to neurological or neurodegenerative disorders.

Preprints (www.preprints.org) | NOT PEER-REVIEWED | Posted: 2 August 2022 doi:10.20944/preprints202208.0045.v1

Pathological mutations in ATAD3A and 17-beta-HSD10 have been previously reported [38,39] and we thus wanted to confirm their ability to interact with SFXN1. With this aim, we analyzed by immunoblot the presence of ATAD3A and 17β-HSD10 in SFXN1 immunoprecipitates (SFXN1-IP). ATAD3A and 17β-HSD10 were specifically detected in the SFXN1-IP in all the cell lines tested, while ATP5b is not detected, confirming the relevance of the MS/MS analysis (**Figure 9a and A5**). Additionally, a proximity ligation assay confirmed the close vicinity of SFXN1 and 17β-HSD10 (**Figure 9b**). TIM50 and NDUFA10 were also confirmed as SFXN1 physical partners.

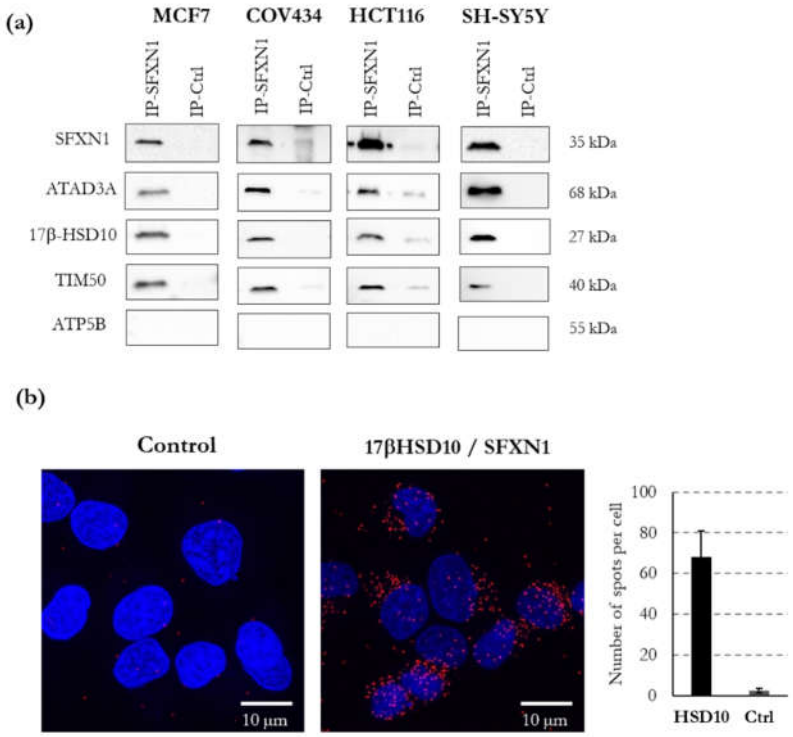

Figure 9: ATAD3, HSD10 and TIM50 are physical partners of SFXN1. (**a**) CoIP of ATAD3A, 17β-HSD10 and TIM50 using an anti-SFXN1 antibody on mitochondrial enriched fractions of MCF7, COV434, HCT116 and SH-SY5Y cells. An isotypic control (rabbit IgG) was used to ensure the specificity of the SFXN1 coIP. No coIP of the β subunit of the F1F0 ATPase (ATP5B) was seen and thus serves as a negative control. (**b**) Proximity ligation assay showing the physical vicinity of SFXN1 and 17β-HSD10 in MCF7 cells (red dots). Signal quantification regarding the control condition is reported on the right panel. Two independent experiments gave similar results. Scale bar: 10 µm.

4. Discussion

SFXN are mitochondrial carriers that are emerging as main actors of OCM and iron metabolism but their precise functions remain unclear. Whereas SFXN1 was recently identified as the mitochondrial transporter of serine, it may also import other amino acids (neutral aminoacids such as Ala, Cys and Gly) or metabolites inside the mitochondria [17]. In this study, we investigated SFXN1 interactome by an experimental approach based on mass spectrometry analysis of coimmunoprecipitated proteins followed by a *in silico* analysis of the candidates. To our knowledge, our study is the first one focusing on the identification of SFXN1 physical partners. In agreement with evidence for a regulation of mitochondrial respiration by sideroflexins [6,16,19], we identified some subunits of the mitochondrial electron transfer chain. Moreover, a physical interaction between SFXN1 and ATAD3A, 17β-HSD10 and TIM50 was further confirmed using different human cell lines.

 doi:10.20944/preprints202208.0045.v1

4.1. Biological processes linked to SFXN1 interactome

Here, we identified mitochondrial organization, mitochondrial transport and mitochondrial respiration as the main biological processes linked to SFXN1 interactome. This does not seem very surprising since SFXN1 is inserted in the inner mitochondrial membrane and probably in the close vicinity of key functional complexes such as respiratory complexes. Thus, we do not exclude the hypothesis of a co-precipitation of members of respiratory complexes because of their physical proximity with SFXN1. Whether SFXN1 directly interacts with some subunits of the respiratory complexes needs to be further investigated. Nevertheless, several studies reported a regulatory role for sideroflexins in mitochondrial respiration based on experiments with KO cells (for review see [3]). In agreement with these studies, we observed that the knockdown of SFXN1 in MCF7 cells impaired the basal and maximal OCR, implying defective mitochondrial respiration (**Figure A8)**. Thus, SFXN1 levels must be tighly controlled to maintain mitochondrial respiration. Previously, we reported a slight increase in iron mitochondrial levels that may be the consequence of a defective heme or iron-sulfur cluster biosynthesis, two cofactors found in some subunits of the respiratory chain. Thus, we wondered if some regulators of iron homeostasis co-precipitated with SFXN1. Over the 83 proteins related to iron ion homeostasis in PANTHER only the sideroflexins SFXN1-5, that were annotated as putative transporters of a metabolite involved in iron homeostasis, were found in SFXN1-IP (**Table B3**). Since late 2018, SFXN1 is known as the mitochondrial transporter of serine and, SFXN2, SFXN3 and SFXN5 may also assume this function [17].

4.2. SFXN1 may interact with the other members of the Sideroflexin family

Whether SFXN1 interacts with others SFXN to form multimers remains an open question. This possibility cannot be excluded since several examples of amino acid transporters functioning as heterodimer exist, such as the system x_{c^-} (a Cys-Glu antiport). Nevertheless, it is also possible that our SFXN1 antibody was able to interact with SFXN2, SFXN3, SFXN5 and to a less extent with SFXN4 under native conditions. Hence, the place of each SFXN in the list of the proteins identified by mass spectrometry is in accordance with their degree of similarity with SFXN1, SFXN3 being the most closely related and SFXN4 the most divergent one. Nevertheless, the question of the multimerization of SFXN merits attention as SFXN1 was recently shown to form a complex of 130 kDa in a BN-PAGE analysis of mitochondria isolated from HEK human cells [40].

4.3. SFXN1, ATAD3A and 17β-HSD10

Here, we identified ATAD3A and 17β-HSD10 as physical interactors of SFXN1. ATPase family AAA domain-containing protein 3 A (ATAD3A) is a mitochondrial transmembrane protein playing a key role in the maintenance of the mitochondria - endoplasmic reticulum (ER) contacts and regulating mitochondrial biogenesis and dynamics [41]. ATAD3A associates with different components of the inner membrane, including OXPHOS complex I and prohibitin complexes [42]. Our results suggest that ATAD3A and SFXN1 belong to the same multimeric complexes. Mutations in the *ATAD3* human gene cluster were reported to cause neurological disorders (Harel-Yoon syndrome, OMIM entry # 617183) and cerebellar disorders [38,43]. Its loss in mouse conditional knockout models leads to severe brain defects [42]. Interestingly, ATAD3 depletion in worms induces mitochondrial iron accumulation and alters the expression of iron regulatory genes [44]. A mitochondrial iron overload has been also reported as a consequence of *SFXN2* or *SFXN4* gene knockout [44] and we previously observed a slight increase in mitochondrial iron levels when SFXN1 levels are decreased by RNA interference [3]. Whether ATAD3 and SFXN1 participate in the same pathways merit to be further investigated.

 doi:10.20944/preprints202208.0045.v1

17β-HSD10 (also known as 3-hydroxyacyl-CoA dehydrogenase type-2, ERAB, ABAD or MRPP2) is a multifunctional NAD(+)-dependent dehydrogenase involved in the biosynthesis of steroids and neurosteroids in the mitochondrial matrix [45]. It is also one of the 3 subunits of the mt-RNAse P complex essential for the maturation of mitochondrial RNA. Pathological mutations in 17β-HSD10 were described in a X-linked disorder [39] (HSD10 mitochondrial disease, OMIM entry # 300438). 17β-HSD10 may also be involved in AD through its interaction with the β-amyloid peptide or its role in neuroactive steroids metabolism [46,47]. In agreement with our findings, a physical interaction between SFXN1 and 17β-HSD10 was previously reported in Liu *et al*, thus reinforcing the hypothesis of a close proximity between SFXN1 and 17β-HSD10. It will thus be interesting to further investigate the relationships between 17β-HSD10 and SFXN1. More specifically, whether SFXN1 is able to regulate 17β-HSD10 functions *i.e*. steroid biosynthesis and mt-RNA maturation remains an open question.

4.4. Physical interaction between SFXN1 and mitochondrial translocases

As the nearly 1500 nuclear-encoded proteins that are targeted to mitochondria, SFXN are synthesized on cytosolic ribosomes. Mitochondrial proteins are imported through one of the five protein import pathways depending of their sequence, structure and final location inside the mitochondrion [30]. The Translocase of the Outer Membrane (TOM) - the main entry door for the mitochondrially targeted proteins - consists of the Tom40 channel associated with several subunits including the receptors Tom20, Tom22 and Tom70. Once translocated through the TOM complex, IMM proteins are then directed to their final destination either by the TIM22 or the TIM23 complex. The TIM22 complex preferentially delivers multi-spanning transmembrane proteins with internal targeting signals to the IMM, such as the metabolite transporters of the SLC25A family, whereas the TIM23 complex is rather dedicated to the translocation of IMM proteins containing a cleavable presequence [48,49]. The human TIM22 complex consists of the Tim22 subunit forming the channel, several chaperones of the IMS shuttling between the TOM and TIM22 complex (namely hTim9, hTim10, hTim10b), Tim29 [49] and AGK (Acylglycerol Kinase) [50,51]. In humans, the TIM23 complex consists of the channel made of the TIM17A/B and TIM23 subunits, the receptor TIM50 and several other proteins. Recent studies highlight the role of AGK in the mitochondrial import of SFXN1, in agreement with its IMM insertion via the TIM22 complex, as expected for a mitochondrial metabolite carrier [19,52]. In our coIP-MS/MS experiment, we have identified TOM22, the central receptor of the TOM complex [53], but neither TOM 20 (the receptor for presequence-containing proteins) nor TOM70 (the preferential receptor for IMS carriers), perhaps because of a too transient interaction. Whereas it is not surprising to find TOM22 in our list of SFXN1-co-precipitated proteins since metabolite carriers enter mitochondria by this route, the presence of TIM50 and TIM17a is rather astonishing since they are implicated in the TIM23 complex but not in the TIM22 complex which ensures the import of multi-spanning proteins and metabolite carriers of the IMS. Because TOM22 and TIM50 can physically interact [54], we favor the hypothesis that we have immunoprecipitated a SFXN1-TOM22 complex containing TIM50 and TIM17A as indirect physical partners of SFXN1. Nevertheless, no component of the TIM22 complex specifically co-precipitated with SFXN1 in this study. One explanation could be that the epitope recognized by our immunoprecipitating antibody is masked when SFXN1 interacts with subunits of the TIM22 complex upon is translocation in the IMM.

4.5. Other partners

Here, we focused on ATAD3A and17β-HSD10, but other candidates with a high Mascot's score also merits our attention. Indeed, the interaction between SFXN1 and the microsomal glutathione S-transferase MGST1, a detoxification enzyme belonging to the Membrane Associated Proteins in Eicosanoid and Glutathione Metabolism

 doi:10.20944/preprints202208.0045.v1

(MAPEG) superfamily [55], could be further investigated. MGST1, an essential enzyme for development and hematopoietic differentiation [56], possesses a lipid peroxidase activity, as GPX4, the main regulator of ferroptosis. Excess iron, as can be seen upon downregulation of SFXN, may trigger oxidative stress eventually leading to a ferroptotic cell death if lipid peroxides are not detoxified by enzymes with glutathione peroxidase activity [57]. SFXN1, as the mitochondrial transporter of Ser may also indirectly participate in the biosynthesis of glutathione (tripeptide γ−L-Glu-L-Cys-Gly), allowing the import of serine in mitochondria and its catabolism by the SHMT2 enzyme, thereby releasing Gly. Functional significance of the SFXN1 – MGST1 interaction observed in this study remains to be documented.

Previously, connexin32 and SCIRR69 were identified as physical partners of SFXN1 [58,59]. These proteins were not found in our list of partners. This could be related to methodological differences (basal or stress conditions for example) or cell-type specific interactions.

5. Conclusions

SFXN1 physical interactants identified here permit to link SFXN1 to complex I and complex IV suggesting that SFXN1 is in the vicinity of respiratory complexes. SFXN4 was recently shown to act as an assembly factor for the complex I interacting with the mitochondrial complex I intermediate assembly (MCIA) which contains TMEM126B [60]. Amongst SFXN1 partners we identified, TMEM126A and TIMMDC1 are two complex I assembly factors interacting with MCIA [61,62]. Thus, it could be interesting to further investigate the role of SFXN1 in regulating complex I assembly. Whether SFXN proteins are able to form multimers is also an open question, since we and others found SFXN1 homologues in the SFXN1 interactome. Finally, in this study, we provide strong evidence for the interaction of SFXN1 with ATAD3A, and with 17β-HSD10. However further work is needed to understand the significance of these physical interactions and to shed light on the role of SFXN1 in neuronal pathophysiology.

Author Contributions: Conceptualization and methodology, N.T., M.B, S.B. and N.L.; investigation and validation, N.T, M.B., A.G., J.D.L.H.; writing—original draft preparation, N.T, M.B., N.L.; writing—review and editing, all authors; funding acquisition, I.G., B.M. and N.L. All authors have read and agreed to the published version of the manuscript.

Funding: This research was partly funded by Agence Nationale de la Recherche (ANR), grant number ANR-21-CE13-0009-01 (SiFeMi project) and NeurATRIS ANR-11-INBS-00110, of the French Investissements d'Avenir Program run by the Agence Nationale pour la Recherche.

Data Availability Statement: Proteomics data are available via ProteomeXchange with identifier PXD030749. The data that support the findings of this study are available from the corresponding author, N.L.F., upon reasonable request

Acknowledgments: We are grateful to Christine Wintz for technical assistance with Drosophila models and Christophe Iochem (Agilent technologies) for its help with Seahorse experiments.

Conflicts of Interest: The authors declare no conflict of interest.

Preprints (www.preprints.org) | NOT PEER-REVIEWED | Posted: 2 August 2022 doi:10.20944/preprints202208.0045.v1

Appendix A: Supplementary figures

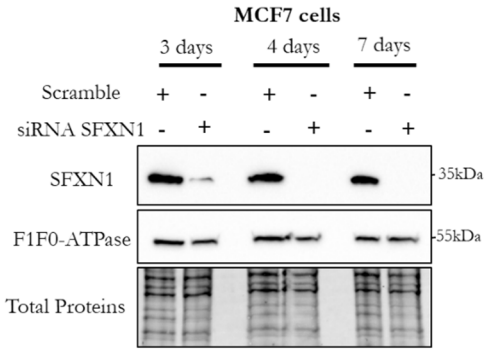

Figure A1: Specificity of the anti-SFXN1 antibody used for immunoblotting. MCF7 cells were transfected with a pool of SFXN1 siRNA (sc-91814, Santa Cruz Biotechnology) and protein extracts were prepared at 3-, 4- and 7-days post-transfection. SFXN1 levels were assessed by western blot using a rabbit anti-SFXN1 antibody (Sigma-Aldrich Cat# HPA019543, RRID:AB_1856789). The ATP5b subunit of the F1FO-ATPase is used as a loading control. Stain-free detection of total proteins is also shown.

Preprints (www.preprints.org) | NOT PEER-REVIEWED | Posted: 2 August 2022 doi:10.20944/preprints202208.0045.v1

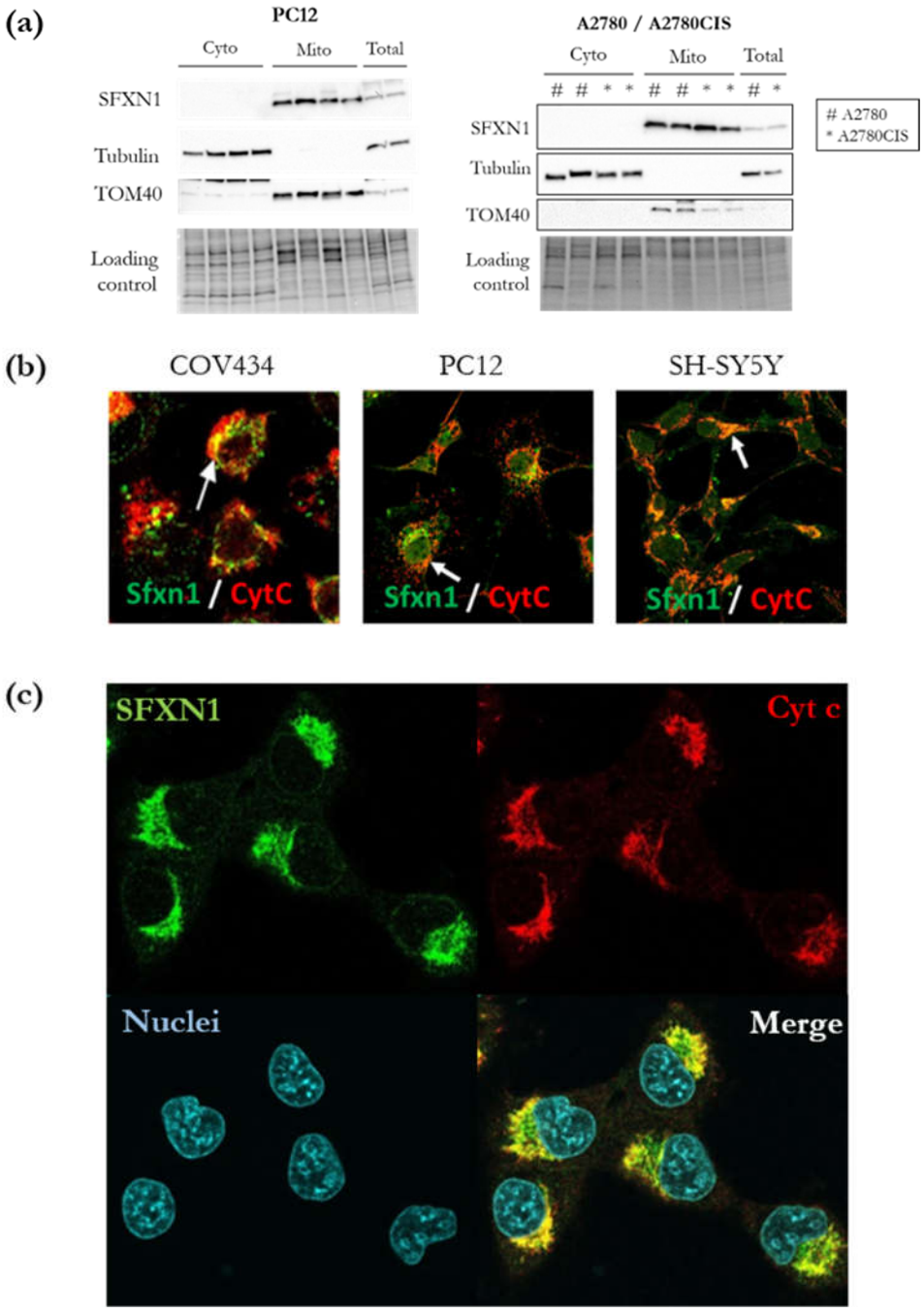

Figure A2: SFXN1 is a mitochondrial protein. (**a**). SFXN1 is detected in mitochondria-enriched fractions from A2780, A2780CIS and PC12 cells but not in cytosolic fractions. Western blot analysis of SFXN1 levels was done with a rabbit specific anti-SFXN1 antibody (Sigma-Aldrich Cat# HPA019543, RRID:AB_1856789). TOM40 is shown to check the purity of the cytosolic fractions. As expected, Tubulin is only detected in cytosolic fractions proving the absence of contamination of the mitochondrial fraction by cytosolic proteins. (**b**). SFXN1 colocalizes with cytochrome c in COV434, PC12 and SH-SY5Y. Immunostaining was done with a rabbit specific anti-SFXN1 antibody (Sigma-Aldrich Cat# HPA019543, RRID:AB_1856789) and images were acquired by confocal fluorescence imaging. (**c**) Immunodetection of SFXN1 and Cytochrome c (mitochondrial staining) in MCF7 cells. A representative image obtained by confocal imaging is shown.

Preprints (www.preprints.org) | NOT PEER-REVIEWED | Posted: 2 August 2022 doi:10.20944/preprints202208.0045.v1

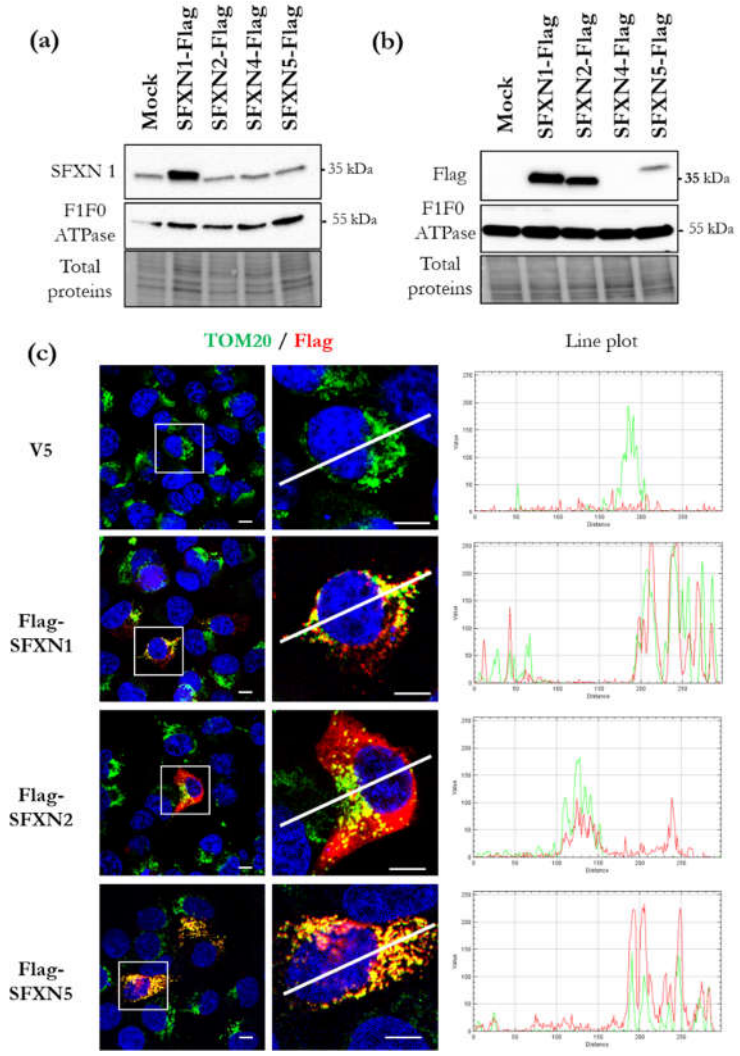

Figure A3: Flag-tagged SFXN1, SFXN2 and SFXN5 proteins colocalize with mitochondria. (**a,b**) Transient transfection of HEK293 cells with SFXN expression vectors (Genscript). HEK293 cells were transiently transfected with an empty vector or plasmids encoding FLAG-tagged SFXN1, SFXN2, SFXN4 or SFXN5. Western blot analysis was done using a polyclonal anti-SFXN1 antibody or an anti-Flag antibody. Total protein amount was observed using stain free labeling before SFXN1, FLAG and F1F0-ATPase revelation. (**c**) Immunofluorescence assay on MCF7 cells transfected with V5 tag or with different Flag-SFXNs. Cells were stained for TOM20 (green) and exogenous SFXNs using anti-FLAG antibody (red). The fluorescence intensities along the lines are show as line profile graphs. Scale Bar= 10 µm.

Preprints (www.preprints.org) | NOT PEER-REVIEWED | Posted: 2 August 2022 doi:10.20944/preprints202208.0045.v1

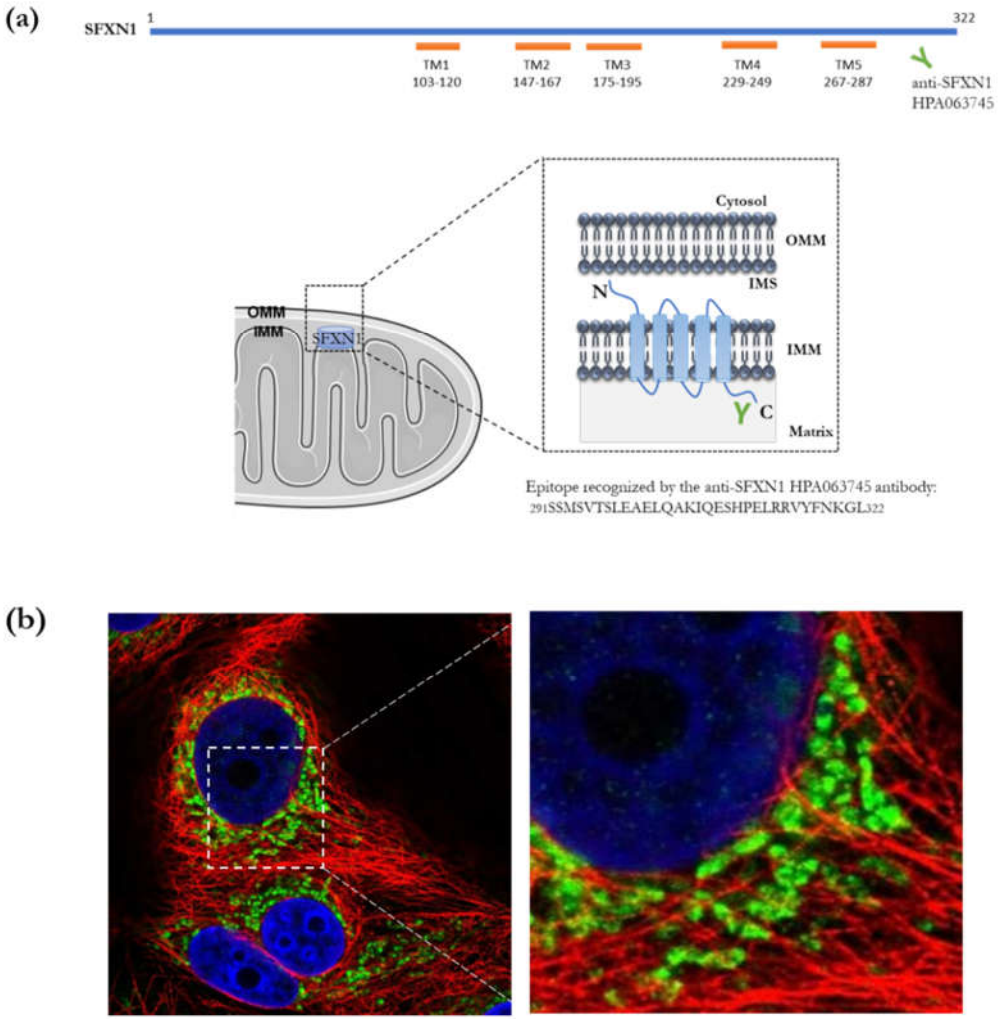

Figure A4: Immunostaining of MCF7 cells with the HPA063745 antibody reveals a mitochondrial pattern. (a) Scheme of human SFXN1 protein (1-322 amino acids) and its topology. The orange bars correspond to the transmembrane helix (TM). The epitope recognized by the Atlas Antibody HPA063745 (Sigma-Aldrich) is present at the C-terminus of the SFXN1 protein (aa291-322, SSMSVTSLEAELQAKIQESHPELRRVYFNKGL) predicted to be in the intermembrane space of the mitochondrion. (b) Immunostaining of MCF7 cells with the HPA063745 antibody reveals spots presumed to be mitochondria. Image credit: Human Protein Atlas available from http://www.proteinatlas.org, image 63745/SFXN1/IF available from version v19.2.proteinatlas.org. Cells were stained using an anti-SFXN1 antibody (green), anti-microtubules antibody (red). Nuclei are stained in blue (DAPI). Scale bar:10μm.

Preprints (www.preprints.org) | NOT PEER-REVIEWED | Posted: 2 August 2022 doi:10.20944/preprints202208.0045.v1

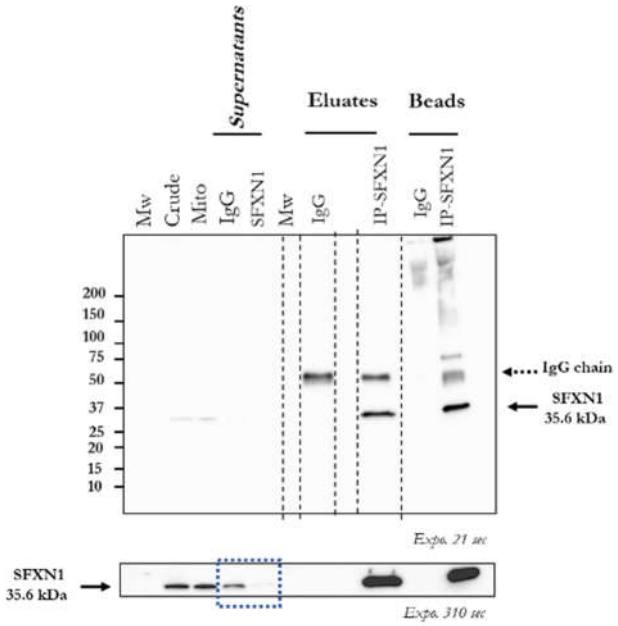

Figure A5: SFXN1 is successfully immunoprecipitated from mitochondria-enriched fractions from MCF7 cells using a specific antibody recognizing its C-terminus (Atlas Antibody HPA063745, Sigma-Aldrich). An isotypic control (anti-Rabbit IgG 12-370, Merck Millipore) was used to show the specificity of SFXN1 IP. After two rounds of elution, beads were conserved and loaded to control the efficiency of elution. Note that a non-neglectable amount of protein remained on the beads. A longer exposure is provided to show the depletion of SFXN1 in supernatants from SFXN1 IP compared to control IgG IP.

Preprints (www.preprints.org) | NOT PEER-REVIEWED | Posted: 2 August 2022 doi:10.20944/preprints202208.0045.v1

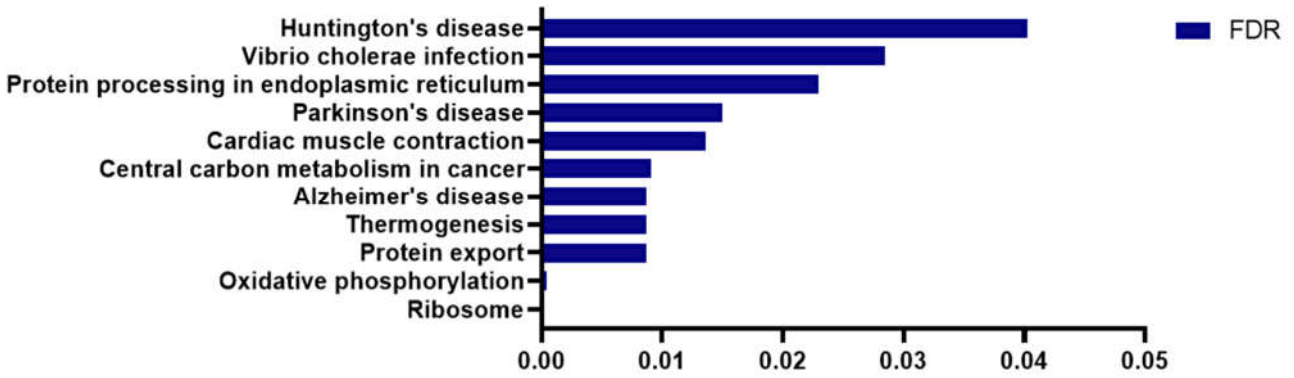

Figure A6: Analysis of STRING v11.0 generated-SFXN1 interactome reveals pathways linked to ribosome and OXPHOS. KEGG pathways with a false discovery rate below 0.05 were listed.

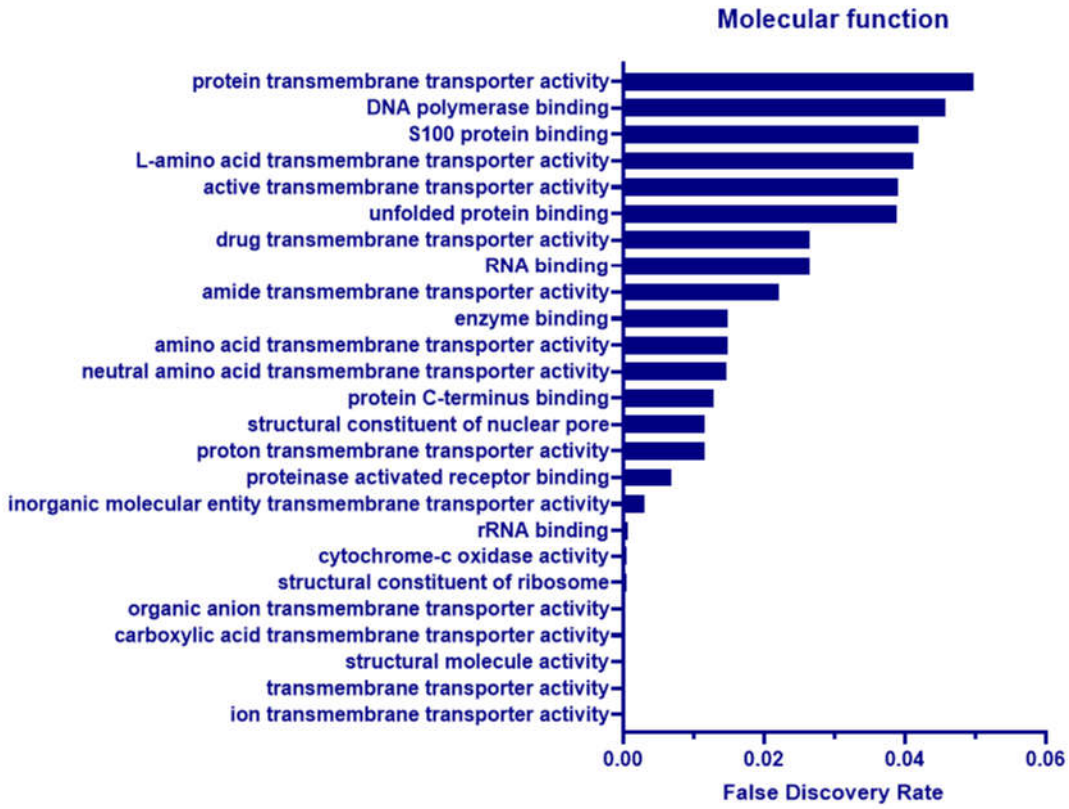

Figure A7: Analysis of STRING v11.0 generated-SFXN1 interactome reveals molecular functions linked to transporter activity, COX activity and RNA binding. Molecular functions linked to SFXN1 physical partners are listed according to the FDR value.

Preprints (www.preprints.org) | NOT PEER-REVIEWED | Posted: 2 August 2022 doi:10.20944/preprints202208.0045.v1

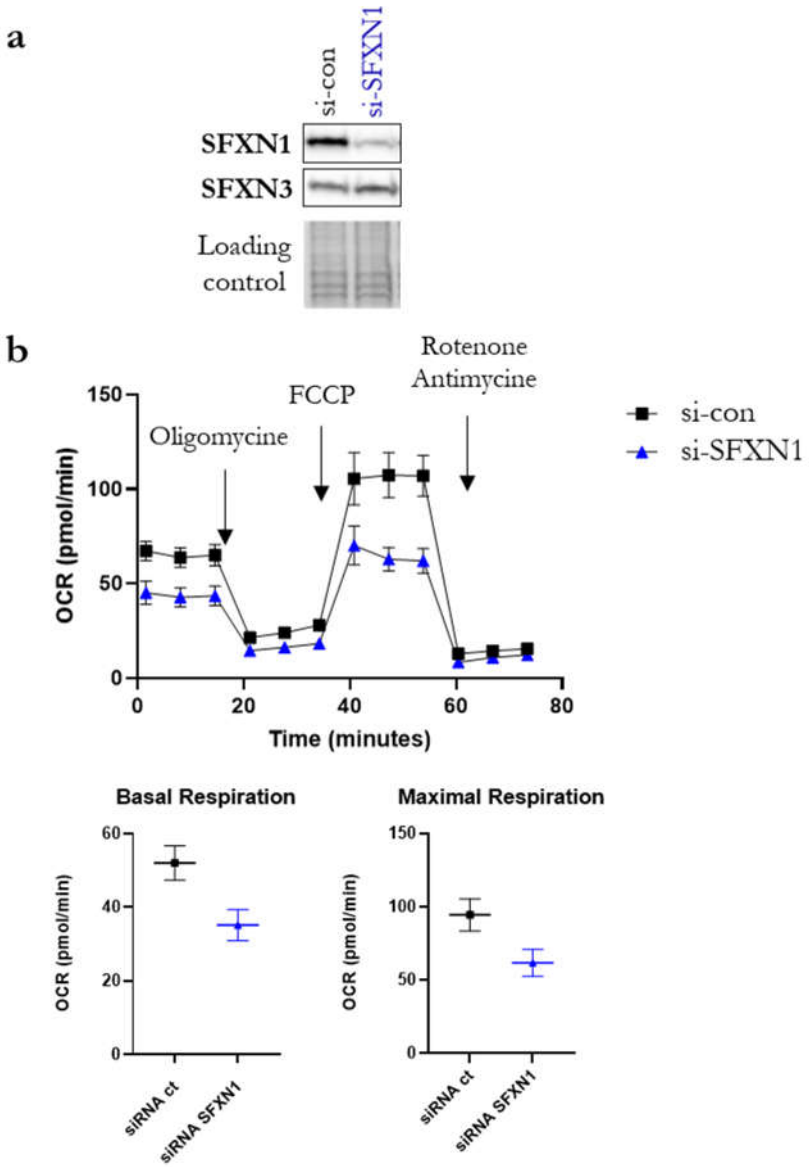

Figure A8: Knockdown of SFXN1 in MCF7 cells impairs mitochondrial respiration. (**a**) Validation of SFXN1 knockdown by Western blot. SFXN3 was detected to ensure the specificity of the SFXN1 siRNA. si-con: scrambled sequence; si-SFXN1: pool of 3 siRNA targeting SFXN1 transcripts. Stain free detection of proteins serves as a loading control. (**b**) Seahorse experiment to monitor oxygen consumption rate of transiently transfected MCF7 cells (Mito Stress Test, Agilent).

Preprints (www.preprints.org) | NOT PEER-REVIEWED | Posted: 2 August 2022 doi:10.20944/preprints202208.0045.v1

Appendix B: Supplementary tables

Table B1. Proteins identified by MS/MS in SFXN1 IP

Name	#Pept [1]	#PSM[2]	Score	Name	#Pept	#PSM	Score
Sideroflexin-1	11	17	605	CD98	1	1	39
Sideroflexin-3	10	11	367	Delta(6) desaturase	2	2	38
Sideroflexin-2	5	7	328	XLalphas	2	2	38
Vimentin	9	10	224	hnRNP M	1	1	38
MGST1	2	3	169	Desmoyokin	1	1	37
ATAD3A	5	5	124	COX6A1	1	1	36
Sideroflexin-5	2	2	123	RAB2B	2	2	36
GLUT-1	1	2	113	HSP 75	1	1	36
KCP-2	2	2	109	TMEM33	1	1	35
MRP-L12	1	1	96	Nucleoporin Nup205	1	1	35
17-beta-HSD 10	3	4	95	LPLAT 7	1	1	34
ValRS	2	2	94	PISD	1	1	34
hLAT1	1	1	89	SMARCA1	1	1	33
MPC2	1	1	89	Prohibitin-2	1	1	33
PIP5K1A-PSMD4	1	1	87	MFTC	1	1	33
Tropomodulin-3	1	2	84	COX11	1	1	33
RCF1b	1	1	81	Zinc finger protein 281	1	1	32
ELOVL FA elongase 1	1	1	78	DAD-1	1	2	32
Nucleoporin Nup160	1	1	77	HSP86	1	1	32
MP68	1	2	75	TIM50	1	1	32
TIMMDC1	1	1	75	Dysferlin	1	1	31
Nrap	1	1	75	COX6C	1	1	30
COMTD1	1	1	75	TRIP-12	1	1	30
IMP-1	1	1	74	Prohibitin	2	2	30
SMIM7	1	1	73	TMEM126A	1	1	29
RPS17	2	2	67	DNA-PKcs	2	2	28
Tim17a	1	1	65	Hp95	1	1	28
EXOC1	1	1	63	UFL1	1	1	28
Sec61 alpha-1	1	1	63	Dnj3	1	1	27
ATP6V0C	1	1	60	MCT 4	1	1	27
SPC22/23	1	1	56	Cytokeratin-10	1	2	26
TMEM209	1	1	55	Beta-III spectrin	1	1	26
N-acetyltransferase 10	1	1	55	ATB(0)	1	1	25
Nudix motif 8	1	1	54	hPAST1	2	2	25
COX7A2	1	1	51	MRM3	1	1	25
Fetuin-A	1	1	50	TMEM111	1	1	24
MTP18	1	1	49	Nucleoporin Nup358	1	1	23
CAS	1	1	49	SCY1-like protein 1	1	1	23
MT-ND2	1	1	48	Alpha1-adaptin	1	1	20
hTom22	1	1	48	SKAP	1	1	20
LMN2R	1	1	48	Alpha-II spectrin	1	1	20
MTA1-L1 protein	1	1	46	DEAD box protein 39	1	1	19
Plectin	2	2	46	SERCA2	1	1	19
Coronin-1C	1	1	44	BiP	1	1	18
MYH-1c	1	1	43	RPS14	1	2	17
NDUFA10	1	1	43	SLC25A12	1	1	16
Ras-like protein TC21	2	2	43	**Sideroflexin-4**	1	1	15
Surfeit locus protein 4	2	2	43	Dystonin	1	1	14
Apoptosis inhibitor 5	1	1	41				

[1] Pept corresponds to the number of distinct peptide sequences. [2] PSM corresponds to the total number of identified peptide sequences for a protein.

 doi:10.20944/preprints202208.0045.v1

Table B2. Biological processes related to the SFXN1 using PANTHER.
Table showing the total number of proteins in each biological process (#Group), the number of binding partners identified (#Identified), the fold enrichment, the P value and the false discovery rate

GO biological process complete	#Group	#Identified	Fold Enrichment	+/-	raw P value	FDR
mitochondrion organization	438	13	6.44	+	1.46E-07	2.55E-04
intracellular protein transport	937	18	4.17	+	3.01E-07	4.29E-04
electron transport chain	176	7	8.63	+	2.17E-05	1.41E-02
establishment of protein localization to organelle	414	10	5.24	+	2.52E-05	1.58E-02
iron ion homeostasis	83	5	13.07	+	5.32E-05	2.77E-02
L-alpha-amino acid transmembrane transport	44	4	19.72	+	6.94E-05	3.51E-02
mitochondrial transmembrane transport	89	5	12.19	+	7.29E-05	3.57E-02
cellular component biogenesis	2666	27	2.20	+	8.12E-05	3.74E-02
protein import	158	6	8.24	+	1.10E-04	4.78E-02

Preprints (www.preprints.org) | NOT PEER-REVIEWED | Posted: 2 August 2022 doi:10.20944/preprints202208.0045.v1

Table B3. Proteins identified in each biological process.

Proteins related to the binding partners of SFXN1 with a FDR below 0.05. The potential binding partners of SFXN1 have been analyzed with the online PANTHER classification system using the PANTHER Overrepresentation test (Released 20171205) and the Gene ontology biological process complete data set.

mitochondrion organization
Tim17a
Prohibitin
COX7A2
MTP18
TIM50
TIMMDC1
17-beta-HSD 10
hTom22
Prohibitin-2
NDUFA10
HSP86
ATAD3A
MT-ND2
intracellular protein transport
RPS14
RPS17
IMP-1
Nrap
Tim17a
Nucleoporin Nup358
DEAD box protein 39
hPAST1
TIM50
Nucleoporin Nup205
Alpha1-adaptin
RAB2B
Nucleoporin Nup160
hTom22
Sec61 alpha-1
Prohibitin-2
SPC22/23
HSP86
electron transport chain
SLC25A12
COX6C
COX7A2
COX6A1
COX11
NDUFA10
MT-ND2
establishment of protein localization to organelle
RPS14
RPS17
Tim17a
Nucleoporin Nup358
TIM50
hTom22
Sec61 alpha-1
Prohibitin-2
SPC22/23
HSP86

iron ion homeostasis
Sideroflexin-1
Sideroflexin-3
Sideroflexin-4
Sideroflexin-2
Sideroflexin-5
L-alpha-amino acid transmembrane transport
SLC25A12
CD98
ATB(0)
hLAT1
mitochondrial transmembrane transport
Tim17a
SLC25A12
MPC2
TIM50
MFTC
cellular component biogenesis
MRM3
RPS14
RPS17
IMP-1
Nrap
hPAST1
CAS
COX7A2
Beta-III spectrin
MYH-1c
N-acetyltransferase 10
TIMMDC1
Nucleoporin Nup205
MGST1
Cytokeratin-10
17-beta-HSD 10
ATB(0)
COX11
Tropomodulin-3
Plectin
Desmoyokin
NDUFA10
Dystonin
GLUT-1
HSP86
Hp95
MT-ND2
protein import
Tim17a
Nucleoporin Nup358
TIM50
hTom22
Prohibitin-2
HSP86

 doi:10.20944/preprints202208.0045.v1

Table B4. Biological pathways related to the SFXN1 binding partners using REACTOME.

Pathways related to the binding partners of SFXN1 with a FDR below 0.05 using REACTOME. After data analysis 29 proteins have not been found.

	#Group	#Identified	pValue	FDR
The citric acid (TCA) cycle and respiratory electron transport	175	9	3,00E-05	7.27E-3
Respiratory electron transport	101	7	3.75E-5	7.27E-3
Respiratory electron transport, ATP synthesis by chemiosmotic coupling, and heat production by uncoupling proteins.	124	7	1.34E-4	1.72E-2
Caspase-mediated cleavage of cytoskeletal proteins	12	3	1.84E-4	1.79E-2

Preprints (www.preprints.org) | NOT PEER-REVIEWED | Posted: 2 August 2022 doi:10.20944/preprints202208.0045.v1

Table B5. List of the antibodies used in this study

Antibodies	Clonality	Host Organism	Dilution	RRID	Provider
Primary antibodies					
Anti-SFXN1	polyclonal	rabbit	1:1000	Sigma-Aldrich Cat# HPA019543, RRID:AB_1856789	Sigma
Anti-SFXN1	polyclonal	rabbit	1:1000	Atlas Antibodies Cat# HPA063745, RRID:AB_2685111	Sigma
Anti-SFXN3	polyclonal	rabbit	1:1000	Atlas Antibodies Cat# HPA048105, RRID:AB_2680265	Sigma
OctA-Probe (H-5) antibody	monoclonal	mouse	1:200	Santa Cruz Biotechnology Cat# sc-166355, RRID:AB_2017593	Santa Cruz
Anti-Mitochondrial ATP Synthase Subunit Beta (ATP5b)	monoclonal	mouse	1:1000	Abcam Cat# ab14730, RRID:AB_301438	Abcam
Anti-ATAD3A/B/C	monoclonal	mouse	1:200	Santa Cruz Biotechnology Cat# sc-376185, RRID:AB_10988379	Santa Cruz
Anti-ERAB (17b-HSD10)	monoclonal	mouse	1:200	Santa Cruz Biotechnology Cat# sc-136326, RRID:AB_10647087	Santa Cruz
Anti-Cytochrome C	monoclonal	mouse	1:1000	BD Biosciences Cat# 556432, RRID:AB_396416	BD Biosciences
Anti-TOM40	polyclonal	rabbit	1:200	Santa Cruz Biotechnology Cat# sc-11414, RRID:AB_793274	Santa Cruz
Anti-TOM20	polyclonal	rabbit	1:200	Santa Cruz Biotechnology Cat# sc-11415, RRID:AB_2207533	Santa Cruz
Anti-Tubulin beta	monoclonal	mouse	1:200	Cat# E7, RRID:AB_528499	DSHB
Anti-Tim50	monoclonal	mouse	1:200	Santa Cruz Biotechnology Cat# sc-393678, RRID:AB_2714191	Santa Cruz
Anti-NDUFA10	monoclonal	mouse	1:200	Santa Cruz Biotechnology Cat# sc-376357, RRID:AB_10990305	Santa Cruz
Secondary antibodies					
Rabbit Normal IgG Control antibody, Unconjugated	polyclonal	rabbit		Millipore Cat# 12-370, RRID:AB_145841	Millipore
Mouse Normal IgG Control antibody, Unconjugated, Millipore	polyclonal	mouse		Millipore Cat# 12-371, RRID:AB_145840	Millipore
Peroxidase AffiniPure Goat Anti-Rabbit IgG (H+L)	polyclonal	goat	1:5000	Jackson ImmunoResearch Labs Cat# 111-035-003, RRID:AB_2313567	Jackson
anti-mouse HRP-conjugated secondary antibody	polyclonal	goat	1:20000	Advansta Cat# R-05071-500, RRID:AB_10718209	Advansta
anti-Rabbit AlexaFluor488	polyclonal	goat	1:200	Thermo Fisher Scientific Cat# A-11008, RRID:AB_143165	ThermoFisher scientific
anti-Rabbit AlexaFluor568	polyclonal	goat	1:200	Thermo Fisher Scientific Cat# A-11011, RRID:AB_143157	ThermoFisher scientific
anti-Mouse AlexaFluor568	polyclonal	goat	1:200	Thermo Fisher Scientific, catalog # A-11004, RRID AB_2534072	ThermoFisher scientific

Preprints (www.preprints.org) | NOT PEER-REVIEWED | Posted: 2 August 2022 doi:10.20944/preprints202208.0045.v1

Table B6. Cell lines used in this study

Cells	Cell Line Description:	Provenance	RRID
A2780	Human ovarian carcinoma derived cell line	ECACC, Sigma-Aldrich	ECACC Cat# 93112519, RRID:CVCL_0134
A2780Cis	Cisplatin-resistant human ovarian carcinoma derived cell line	ECACC, Sigma-Aldrich	ECACC Cat# 93112517, RRID:CVCL_1942
COV434	Human ovarian cancer derived cell line	Kind gift from Sandrine Caburet	ECACC Cat# 07071909, RRID:CVCL_2010
HCT116	human colon cancer derived cell line	our lab	CVCL_0291
HEK293	human embryonic kidney 293 cells	our lab	CVCL_0045
HeLa	Human cervical cancer derived cell line	our lab	CVCL_0030
HepG2	Human liver carcinoma derived cell line	Kind gift from Delphine Sitterlin	CVCL_0027
HT1080	Fibrosarcoma derived cell line	our lab	CVCL_0317
KGN	Human granulosa-like tumor derived cell line	Kind gift from Sandrine Caburet	CVCL_0375
MCF-7	Human breast cancer cell line	Kind gift from Philippe Juin	CVCL_0031
MDA-MB-231	Human breast cancer derived cell line	Kind gift from Philippe Juin	CVCL_0062
MDA-MB-468	Human breast cancer derived cell line	Kind gift from Philippe Juin	CVCL_0419
MEFSV40	Mouse immortalized embryonic fibroblasts	Kind from Richard Flavell	CVCL_U630
PC12	Rat derived pheochromocytoma	our lab	CVCL_0481
RKO	Human colon carcinoma derived cell line	our lab	CVCL_0504
SH-SY5Y	Human neuroblastoma derived cell line	ATCC	ATCC Cat# CRL-2266, RRID:CVCL_0019
T-47D	human breast cancer derived cell line	Kind gift from Philippe Juin	CVCL_0553

Table B7. Plasmids used in this study (related to figure A3, purchased from Genscript).

Protein	Cloning vector	Clone ID	Gene symbol	Accession number
SFXN1	pcDNA3.1+/C-(K)-DYK	OHu31628	SFXN1	NM_022754.6
SFXN2	pcDNA3.1+/C-(K)-DYK	OHu14540	SFXN2	NM_178858.5
SFXN4	pcDNA3.1+/C-(K)-DYK	OHu25980	SFXN4	NM_213649.1
SFXN5	pcDNA3.1+/C-(K)-DYK	OHu17388	SFXN5	NM_144579.2

References

1. SLC56 Sideroflexins. IUPHAR/BPS Guide to PHARMACOLOGY 2020.
2. Gyimesi, G.; Hediger, M.A. Sequence Features of Mitochondrial Transporter Protein Families. *Biomolecules* **2020**, *10*, 1611, doi:10.3390/biom10121611.
3. Tifoun, N.; De las Heras, J.M.; Guillaume, A.; Bouleau, S.; Mignotte, B.; Le Floch, N. Insights into the Roles of the Sideroflexins/SLC56 Family in Iron Homeostasis and Iron-Sulfur Biogenesis. *Biomedicines* **2021**, *9*, 103, doi:10.3390/biomedicines9020103.
4. Hildick-Smith, G.J.; Cooney, J.D.; Garone, C.; Kremer, L.S.; Haack, T.B.; Thon, J.N.; Miyata, N.; Lieber, D.S.; Calvo, S.E.; Akman, H.O.; et al. Macrocytic Anemia and Mitochondriopathy Resulting from a Defect in Sideroflexin 4. *Am. J. Hum. Genet.* **2013**, *93*, 906–914, doi:10.1016/j.ajhg.2013.09.011.
5. Tulinius, M.; Kollberg, G.; Darin, N.; Oldfors, A.; Asin-Cayuela, J. Congenital Mitochondrial Encephalomyopathy with Complex I Deficiency Due to Mutations in Sideroflexin 4 (SFXN4). *Neuromuscul. Disord.* **2016**, *26*, S175, doi:10.1016/j.nmd.2016.06.324.
6. Sofou, K.; Hedberg-Oldfors, C.; Kollberg, G.; Thomsen, C.; Wiksell, Å.; Oldfors, A.; Tulinius, M. Prenatal onset of mitochondrial disease is associated with sideroflexin 4 deficiency. *Mitochondrion* **2019**, *47*, 76–81, doi:10.1016/j.mito.2019.04.012.
7. Minjarez, B.; Calderón-González, K.G.; Rustarazo, M.L.V.; Herrera-Aguirre, M.E.; Labra-Barrios, M.L.; Rincon-Limas, D.E.; Del Pino, M.M.S.; Mena, R.; Luna-Arias, J.P. Identification of Proteins That Are Differentially Expressed in Brains with Alzheimer's Disease Using ITRAQ Labeling and Tandem Mass Spectrometry. *J. Proteomics* **2016**, *139*, 103–121, doi:10.1016/j.jprot.2016.03.022.
8. Simunovic, F.; Yi, M.; Wang, Y.; Macey, L.; Brown, L.T.; Krichevsky, A.M.; Andersen, S.L.; Stephens, R.M.; Benes, F.M.; Sonntag, K.C. Gene Expression Profiling of Substantia Nigra Dopamine Neurons: Further Insights into Parkinson's Disease Pathology. *Brain* **2009**, *132*, 1795–1809, doi:10.1093/brain/awn323.
9. Amorim, I.S.; Graham, L.C.; Carter, R.N.; Morton, N.M.; Hammachi, F.; Kunath, T.; Pennetta, G.; Carpanini, S.M.; Manson, J.C.; Lamont, D.J.; et al. Sideroflexin 3 Is an α-Synuclein-Dependent Mitochondrial Protein That Regulates Synaptic Morphology. *J. Cell Sci.* **2017**, *130*, 325–331, doi:10.1242/jcs.194241.
10. Rivell, A.; Petralia, R.S.; Wang, Y.-X.; Mattson, M.P.; Yao, P.J. Sideroflexin 3 Is a Mitochondrial Protein Enriched in Neurons. *NeuroMolecular Med.* **2019**, *21*, 314–321, doi:10.1007/s12017-019-08553-7.
11. Ledahawsky, L.M.; Terzenidou, M.E.; Edwards, R.; Kline, R.A.; Graham, L.C.; Eaton, S.L.; Hoorn, D.; Chaytow, H.; Huang, Y.; Groen, E.J.N.; et al. The Mitochondrial Protein Sideroflexin 3 (SFXN3) Influences Neurodegeneration Pathways *in Vivo*. *FEBS J.* **2022**, febs.16377, doi:10.1111/febs.16377.
12. Chen, B.; Aredo, B.; Ding, Y.; Zhong, X.; Zhu, Y.; Zhao, C.X.; Kumar, A.; Xing, C.; Gautron, L.; Lyon, S.; et al. Forward Genetic Analysis Using OCT Screening Identifies *Sfxn3* Mutations Leading to Progressive Outer Retinal Degeneration in Mice. *Proc. Natl. Acad. Sci.* **2020**, *117*, 12931–12942, doi:10.1073/pnas.1921224117.
13. Kovaleva, G.Yu.; Bazykin, G.A.; Brudno, M.; Gelfand, M.S. COMPARATIVE GENOMICS OF TRANSCRIPTIONAL REGULATION IN YEASTS AND ITS APPLICATION TO IDENTIFICATION OF A CANDIDATE ALPHA-ISOPROPYLMALATE TRANSPORTER. *J. Bioinform. Comput. Biol.* **2006**, *04*, 981–998, doi:10.1142/S0219720006002284.
14. Fleming, M.D. A Mutation in a Mitochondrial Transmembrane Protein Is Responsible for the Pleiotropic Hematological and Skeletal Phenotype of Flexed-Tail (f/f) Mice. *Genes Dev.* **2001**, *15*, 652–657, doi:10.1101/gad.873001.
15. Mon, E.E.; Wei, F.-Y.; Ahmad, R.N.R.; Yamamoto, T.; Moroishi, T.; Tomizawa, K. Regulation of Mitochondrial Iron Homeostasis by Sideroflexin 2. *J. Physiol. Sci.* **2019**, *69*, 359–373, doi:10.1007/s12576-018-0652-2.
16. Paul, B.T.; Tesfay, L.; Winkler, C.R.; Torti, F.M.; Torti, S.V. Sideroflexin 4 Affects Fe-S Cluster Biogenesis, Iron Metabolism, Mitochondrial Respiration and Heme Biosynthetic Enzymes. *Sci. Rep.* **2019**, *9*, 19634, doi:10.1038/s41598-019-55907-z.
17. Kory, N.; Wyant, G.A.; Prakash, G.; uit de Bos, J.; Bottanelli, F.; Pacold, M.E.; Chan, S.H.; Lewis, C.A.; Wang, T.; Keys, H.R.; et al. SFXN1 Is a Mitochondrial Serine Transporter Required for One-Carbon Metabolism. *Science* **2018**, *362*, eaat9528, doi:10.1126/science.aat9528.
18. Ducker, G.S.; Rabinowitz, J.D. One-Carbon Metabolism in Health and Disease. *Cell Metab.* **2017**, *25*, 27–42, doi:10.1016/j.cmet.2016.08.009.
19. Acoba, M.G.; Alpergin, E.S.S.; Renuse, S.; Fernández-del-Río, L.; Lu, Y.-W.; Khalimonchuk, O.; Clarke, C.F.; Pandey, A.; Wolfgang, M.J.; Claypool, S.M. The Mitochondrial Carrier SFXN1 Is Critical for Complex III Integrity and Cellular Metabolism. *Cell Rep.* **2021**, *34*, 108869, doi:10.1016/j.celrep.2021.108869.
20. Bao, B.; An, W.; Lu, Q.; Wang, Y.; Lu, Z.; Tu, J.; Zhang, H.; Duan, Y.; Yuan, W.; Zhu, X.; et al. Sfxn1 Is Essential for Erythrocyte Maturation via Facilitating Hemoglobin Production in Zebrafish. *Biochim. Biophys. Acta BBA - Mol. Basis Dis.* **2021**, *1867*, 166096, doi:10.1016/j.bbadis.2021.166096.
21. Manousakidi, S.; Guillaume, A.; Pirou, C.; Bouleau, S.; Mignotte, B.; Renaud, F.; Le Floch, N. FGF1 Induces Resistance to Chemotherapy in Ovarian Granulosa Tumor Cells through Regulation of P53 Mitochondrial Localization. *Oncogenesis* **2018**, *7*, 18, doi:10.1038/s41389-018-0033-y.
22. Schindelin, J.; Arganda-Carreras, I.; Frise, E.; Kaynig, V.; Longair, M.; Pietzsch, T.; Preibisch, S.; Rueden, C.; Saalfeld, S.; Schmid, B.; et al. Fiji: An Open-Source Platform for Biological-Image Analysis. *Nat. Methods* **2012**, *9*, 676–682, doi:10.1038/nmeth.2019.

23. Manders, E.M.M.; Verbeek, F.J.; Aten, J.A. Measurement of Co-Localization of Objects in Dual-Colour Confocal Images. *J. Microsc.* **1993**, *169*, 375–382, doi:10.1111/j.1365-2818.1993.tb03313.x.
24. Aaron, J.S.; Taylor, A.B.; Chew, T.-L. Image Co-Localization – Co-Occurrence versus Correlation. *J. Cell Sci.* **2018**, *131*, jcs211847, doi:10.1242/jcs.211847.
25. Perez-Riverol, Y.; Csordas, A.; Bai, J.; Bernal-Llinares, M.; Hewapathirana, S.; Kundu, D.J.; Inuganti, A.; Griss, J.; Mayer, G.; Eisenacher, M.; et al. The PRIDE Database and Related Tools and Resources in 2019: Improving Support for Quantification Data. *Nucleic Acids Res.* **2019**, *47*, D442–D450, doi:10.1093/nar/gky1106.
26. The Gene Ontology Consortium The Gene Ontology Resource: 20 Years and Still GOing Strong. *Nucleic Acids Res.* **2019**, *47*, D330–D338, doi:10.1093/nar/gky1055.
27. Ashburner, M.; Ball, C.A.; Blake, J.A.; Botstein, D.; Butler, H.; Cherry, J.M.; Davis, A.P.; Dolinski, K.; Dwight, S.S.; Eppig, J.T.; et al. Gene Ontology: Tool for the Unification of Biology. *Nat. Genet.* **2000**, *25*, 25–29, doi:10.1038/75556.
28. Mi, H.; Muruganujan, A.; Ebert, D.; Huang, X.; Thomas, P.D. PANTHER Version 14: More Genomes, a New PANTHER GO-Slim and Improvements in Enrichment Analysis Tools. *Nucleic Acids Res.* **2019**, *47*, D419–D426, doi:10.1093/nar/gky1038.
29. Bandrowski, A.; Brush, M.; Grethe, J.S.; Haendel, M.A.; Kennedy, D.N.; Hill, S.; Hof, P.R.; Martone, M.E.; Pols, M.; Tan, S.; et al. The Resource Identification Initiative: A Cultural Shift in Publishing. *F1000Research* **2015**, *4*, 134, doi:10.12688/f1000research.6555.2.
30. Thul, P.J.; Åkesson, L.; Wiking, M.; Mahdessian, D.; Geladaki, A.; Ait Blal, H.; Alm, T.; Asplund, A.; Björk, L.; Breckels, L.M.; et al. A Subcellular Map of the Human Proteome. *Science* **2017**, *356*, eaal3321, doi:10.1126/science.aal3321.
31. Lee, S.-Y.; Kang, M.-G.; Park, J.-S.; Lee, G.; Ting, A.Y.; Rhee, H.-W. APEX Fingerprinting Reveals the Subcellular Localization of Proteins of Interest. *Cell Rep.* **2016**, *15*, 1837–1847, doi:10.1016/j.celrep.2016.04.064.
32. Szklarczyk, D.; Gable, A.L.; Lyon, D.; Junge, A.; Wyder, S.; Huerta-Cepas, J.; Simonovic, M.; Doncheva, N.T.; Morris, J.H.; Bork, P.; et al. STRING V11: Protein–Protein Association Networks with Increased Coverage, Supporting Functional Discovery in Genome-Wide Experimental Datasets. *Nucleic Acids Res.* **2019**, *47*, D607–D613, doi:10.1093/nar/gky1131.
33. Zhou, Y.; Zhou, B.; Pache, L.; Chang, M.; Khodabakhshi, A.H.; Tanaseichuk, O.; Benner, C.; Chanda, S.K. Metascape Provides a Biologist-Oriented Resource for the Analysis of Systems-Level Datasets. *Nat. Commun.* **2019**, *10*, 1523, doi:10.1038/s41467-019-09234-6.
34. Liu, X.; Salokas, K.; Tamene, F.; Jiu, Y.; Weldatsadik, R.G.; Öhman, T.; Varjosalo, M. An AP-MS- and BioID-Compatible MAC-Tag Enables Comprehensive Mapping of Protein Interactions and Subcellular Localizations. *Nat. Commun.* **2018**, *9*, 1188, doi:10.1038/s41467-018-03523-2.
35. Palmieri, L.; Pardo, B.; Lasorsa, F.M.; del Arco, A.; Kobayashi, K.; Iijima, M.; Runswick, M.J.; Walker, J.E.; Saheki, T.; Satrústegui, J.; et al. Citrin and Aralar1 Are Ca2+-Stimulated Aspartate/Glutamate Transporters in Mitochondria. *EMBO J.* **2001**, *20*, 5060–5069, doi:10.1093/emboj/20.18.5060.
36. Scalise, M.; Pochini, L.; Console, L.; Losso, M.A.; Indiveri, C. The Human SLC1A5 (ASCT2) Amino Acid Transporter: From Function to Structure and Role in Cell Biology. *Front. Cell Dev. Biol.* **2018**, *6*, 96, doi:10.3389/fcell.2018.00096.
37. Yoo, H.C.; Park, S.J.; Nam, M.; Kang, J.; Kim, K.; Yeo, J.H.; Kim, J.-K.; Heo, Y.; Lee, H.S.; Lee, M.Y.; et al. A Variant of SLC1A5 Is a Mitochondrial Glutamine Transporter for Metabolic Reprogramming in Cancer Cells. *Cell Metab.* **2020**, *31*, 267-283.e12, doi:10.1016/j.cmet.2019.11.020.
38. Desai, R.; Frazier, A.E.; Durigon, R.; Patel, H.; Jones, A.W.; Dalla Rosa, I.; Lake, N.J.; Compton, A.G.; Mountford, H.S.; Tucker, E.J.; et al. ATAD3 Gene Cluster Deletions Cause Cerebellar Dysfunction Associated with Altered Mitochondrial DNA and Cholesterol Metabolism. *Brain* **2017**, *140*, 1595–1610, doi:10.1093/brain/awx094.
39. Zschocke, J. HSD10 Disease: Clinical Consequences of Mutations in the HSD17B10 Gene. *J. Inherit. Metab. Dis.* **2012**, *35*, 81–89, doi:10.1007/s10545-011-9415-4.
40. Jackson, T.D.; Hock, D.; Palmer, C.S.; Kang, Y.; Fujihara, K.M.; Clemons, N.J.; Thorburn, D.R.; Stroud, D.A.; Stojanovski, D. *The TIM22 Complex Regulates Mitochondrial One-Carbon Metabolism by Mediating the Import of Sideroflexins*; Biorxiv, 2020;
41. Baudier, J. ATAD3 Proteins: Brokers of a Mitochondria-Endoplasmic Reticulum Connection in Mammalian Cells: Mitochondria-Endoplasmic Reticulum Connection. *Biol. Rev.* **2018**, *93*, 827–844, doi:10.1111/brv.12373.
42. Arguello, T.; Peralta, S.; Antonicka, H.; Gaidosh, G.; Diaz, F.; Tu, Y.-T.; Garcia, S.; Shiekhattar, R.; Barrientos, A.; Moraes, C.T. ATAD3A Has a Scaffolding Role Regulating Mitochondria Inner Membrane Structure and Protein Assembly. *Cell Rep.* **2021**, *37*, 110139, doi:10.1016/j.celrep.2021.110139.
43. Harel, T.; Yoon, W.H.; Garone, C.; Gu, S.; Coban-Akdemir, Z.; Eldomery, M.K.; Posey, J.E.; Jhangiani, S.N.; Rosenfeld, J.A.; Cho, M.T.; et al. Recurrent De Novo and Biallelic Variation of ATAD3A , Encoding a Mitochondrial Membrane Protein, Results in Distinct Neurological Syndromes. *Am. J. Hum. Genet.* **2016**, *99*, 831–845, doi:10.1016/j.ajhg.2016.08.007.
44. van den Ecker, D.; Hoffmann, M.; Müting, G.; Maglioni, S.; Herebian, D.; Mayatepek, E.; Ventura, N.; Distelmaier, F. Caenorhabditis Elegans ATAD-3 Modulates Mitochondrial Iron and Heme Homeostasis. *Biochem. Biophys. Res. Commun.* **2015**, *467*, 389–394, doi:10.1016/j.bbrc.2015.09.143.
45. He, X.-Y.; Isaacs, C.; Yang, S.-Y. Roles of Mitochondrial 17β-Hydroxysteroid Dehydrogenase Type 10 in Alzheimer's Disease. *J. Alzheimers Dis.* **2018**, *62*, 665–673, doi:10.3233/JAD-170974.
46. Aitken, L.; Baillie, G.; Pannifer, A.; Morrison, A.; Jones, P.S.; Smith, T.K.; McElroy, S.P.; Gunn-Moore, F.J. In Vitro Assay Development and HTS of Small-Molecule Human ABAD/17β-HSD10 Inhibitors as Therapeutics in Alzheimer's Disease. *SLAS Discov. Adv. Sci. Drug Discov.* **2017**, *22*, 676–685, doi:10.1177/2472555217697964.

47. Yang, S.-Y.; He, X.-Y.; Isaacs, C.; Dobkin, C.; Miller, D.; Philipp, M. Roles of 17β-Hydroxysteroid Dehydrogenase Type 10 in Neurodegenerative Disorders. *J. Steroid Biochem. Mol. Biol.* **2014**, *143*, 460–472, doi:10.1016/j.jsbmb.2014.07.001.
48. Wiedemann, N.; Pfanner, N. Mitochondrial Machineries for Protein Import and Assembly. *Annu. Rev. Biochem.* **2017**, *86*, 685–714, doi:10.1146/annurev-biochem-060815-014352.
49. Callegari, S.; Richter, F.; Chojnacka, K.; Jans, D.C.; Lorenzi, I.; Pacheu-Grau, D.; Jakobs, S.; Lenz, C.; Urlaub, H.; Dudek, J.; et al. TIM29 Is a Subunit of the Human Carrier Translocase Required for Protein Transport. *FEBS Lett.* **2016**, *590*, 4147–4158, doi:10.1002/1873-3468.12450.
50. Kang, Y.; Stroud, D.A.; Baker, M.J.; De Souza, D.P.; Frazier, A.E.; Liem, M.; Tull, D.; Mathivanan, S.; McConville, M.J.; Thorburn, D.R.; et al. Sengers Syndrome-Associated Mitochondrial Acylglycerol Kinase Is a Subunit of the Human TIM22 Protein Import Complex. *Mol. Cell* **2017**, *67*, 457-470.e5, doi:10.1016/j.molcel.2017.06.014.
51. Vukotic, M.; Nolte, H.; König, T.; Saita, S.; Ananjew, M.; Krüger, M.; Tatsuta, T.; Langer, T. Acylglycerol Kinase Mutated in Sengers Syndrome Is a Subunit of the TIM22 Protein Translocase in Mitochondria. *Mol. Cell* **2017**, *67*, 471-483.e7, doi:10.1016/j.molcel.2017.06.013.
52. Jackson, T.D.; Hock, D.H.; Fujihara, K.M.; Palmer, C.S.; Frazier, A.E.; Low, Y.C.; Kang, Y.; Ang, C.-S.; Clemons, N.J.; Thorburn, D.R.; et al. The TIM22 Complex Mediates the Import of Sideroflexins and Is Required for Efficient Mitochondrial One-Carbon Metabolism. *Mol. Biol. Cell* **2021**, *32*, 475–491, doi:10.1091/mbc.E20-06-0390.
53. Becker, T.; Song, J.; Pfanner, N. Versatility of Preprotein Transfer from the Cytosol to Mitochondria. *Trends Cell Biol.* **2019**, *29*, 534–548, doi:10.1016/j.tcb.2019.03.007.
54. Shiota, T.; Mabuchi, H.; Tanaka-Yamano, S.; Yamano, K.; Endo, T. In Vivo Protein-Interaction Mapping of a Mitochondrial Translocator Protein Tom22 at Work. *Proc. Natl. Acad. Sci.* **2011**, *108*, 15179–15183, doi:10.1073/pnas.1105921108.
55. Kuang, Q.; Purhonen, P.; Ålander, J.; Svensson, R.; Hoogland, V.; Winerdal, J.; Spahiu, L.; Ottosson-Wadlund, A.; Jegerschöld, C.; Morgenstern, R.; et al. Dead-End Complex, Lipid Interactions and Catalytic Mechanism of Microsomal Glutathione Transferase 1, an Electron Crystallography and Mutagenesis Investigation. *Sci. Rep.* **2017**, *7*, 7897, doi:10.1038/s41598-017-07912-3.
56. Bräutigam, L.; Zhang, J.; Dreij, K.; Spahiu, L.; Holmgren, A.; Abe, H.; Tew, K.D.; Townsend, D.M.; Kelner, M.J.; Morgenstern, R.; et al. MGST1, a GSH Transferase/Peroxidase Essential for Development and Hematopoietic Stem Cell Differentiation. *Redox Biol.* **2018**, *17*, 171–179, doi:10.1016/j.redox.2018.04.013.
57. Stockwell, B.R.; Friedmann Angeli, J.P.; Bayir, H.; Bush, A.I.; Conrad, M.; Dixon, S.J.; Fulda, S.; Gascón, S.; Hatzios, S.K.; Kagan, V.E.; et al. Ferroptosis: A Regulated Cell Death Nexus Linking Metabolism, Redox Biology, and Disease. *Cell* **2017**, *171*, 273–285, doi:10.1016/j.cell.2017.09.021.
58. Fowler, S.L.; Akins, M.; Zhou, H.; Figeys, D.; Bennett, S.A.L. The Liver Connexin32 Interactome Is a Novel Plasma Membrane-Mitochondrial Signaling Nexus. *J. Proteome Res.* **2013**, *12*, 2597–2610, doi:10.1021/pr301166p.
59. Chen, Y.; Liu, Y.; Lin, S.; Yang, S.; Que, H.; Liu, S. Identification of Novel SCIRR69-Interacting Proteins During ER Stress Using SILAC-Immunoprecipitation Quantitative Proteomics Approach. *NeuroMolecular Med.* **2017**, *19*, 81–93, doi:10.1007/s12017-016-8431-9.
60. Jackson, T.D.; Crameri, J.J.; Muellner-Wong, L.; Frazier, A.E.; Palmer, C.S.; Formosa, L.E.; Hock, D.H.; Fujihara, K.M.; Stait, T.; Sharpe, A.J.; et al. Sideroflexin 4 Is a Complex I Assembly Factor That Interacts with the MCIA Complex and Is Required for the Assembly of the ND2 Module. *Proc. Natl. Acad. Sci.* **2022**, *119*, e2115566119, doi:10.1073/pnas.2115566119.
61. Formosa, L.E.; Reljic, B.; Sharpe, A.J.; Hock, D.H.; Muellner-Wong, L.; Stroud, D.A.; Ryan, M.T. Optic Atrophy–Associated TMEM126A Is an Assembly Factor for the ND4-Module of Mitochondrial Complex I. *Proc. Natl. Acad. Sci.* **2021**, *118*, e2019665118, doi:10.1073/pnas.2019665118.
62. Guarani, V.; Paulo, J.; Zhai, B.; Huttlin, E.L.; Gygi, S.P.; Harper, J.W. TIMMDC1/C3orf1 Functions as a Membrane-Embedded Mitochondrial Complex I Assembly Factor through Association with the MCIA Complex. *Mol. Cell. Biol.* **2014**, *34*, 847–861, doi:10.1128/MCB.01551-13.